Abstract

Bharadwaj, Arjun. On Quantifying Covertness of Ultra-Wideband Impulse Radio. (Under the direction of Dr. Keith Townsend.)

Impulse Radio (IR) is a time-hopping ultra wideband CDMA communication system that possess unique characteristics which make it a promising candidate for future tactical military radio networks. IR makes a good candidate because of its covertness, low power spectral density and relative immunity to multipath fading.

Beyond qualitative assertions about the performance and covertness of impulse radio, there has not been a thorough quantitative evaluation of the covertness of IR. Thus there is a need for an unclassified quantitative method for defining Low Probability of Detection (LPD) characteristics of a system.

In this thesis, we compare the performance of impulse radio with DS CDMA with and without severe local interferers. Cellular systems are typically narrowband and thus the DS CDMA system was modified so that the spectral characteristics of the chip sequences match the monopulses of impulse radio. We find that the performance of impulse radio is better than DS CDMA for single and multiple users with and without severe local interferers.

We develop a multi-radiometer system ideal for detecting the pulses of impulse radio. A covertness metric (Signal power-to-Noise spectral density) is defined and the detector is used to quantify the covertness of impulse radio. Since the system parameters of impulse radio may be unknown to an interceptor, the covertness is calculated for the ideal case as well as varying amounts of prior knowledge. Single and multiple user cases

with non-overlapping pulses are considered and average covertness is determined for the multiple user overlapping case. The covertness of impulse radio was compared is COTS systems. Results show that impulse radio demonstrated good covertness even when an ideal multi-radiometer detector is used. Covertness of impulse radio was much better than conventional communication systems like IS-95 and wideband CDMA.

An effective network design is essential for taking advantage of the gains of impulse radio. We evaluate the performance and covertness of a peer-to-peer topology with distributed closed loop power control. Saturated links which do not converge to a steady state even at maximum transit powers are eliminated by link level monitoring. Random topologies are generated and capacity bounds determined for networks operating in a simulated geographic area. An acceptable covertness measure was defined and covertness was calculated by network simulations. We found that covertness degrades when link lengths increase due to user mobility. Optimal link lengths for a given number of users and geographic area are specified.

On Quantifying Covertness of Ultra-Wideband Impulse Radio

by

Arjun Bharadwaj

A thesis submitted to the Graduate Faculty of
North Carolina State University
in partial fulfillment of the
requirements for the Degree of
Master of Science

Electrical Engineering

Raleigh, N.C.

August 15, 2002

APPROVED BY:

Dr. Brian Hughes	Dr. Alexandra Duel-Hallen

Dr. J. K. Townsend,
Chair of Advisory Committee

Biography

Arjun Bharadwaj was born on May 18, 1978 in Chennai, India. He completed his schooling at P. S. Senior Secondary School in May 1995. He graduated from Regional Engineering College, Trichy in May 1999 with a bachelors degree in Electronics and Communicatons Engineering. He worked as a communications engineer for RadioCosm from August 2001 to July 2002. He received his M.S in Electrical Engineering from North Carolina State University, in December 2002. His interests are in wireless communication systems.

Acknowledgements

I would like to thank my advisor Dr. Keith Townsend without whose guidance and help this thesis would have but remained a dream. I thank him for his patience and support, his advice and encouragement and his immense tolerance.

Contents

List of Figures

List of Tables

Chapter 1

Introduction

1.1 Motivation

Military operations today include a mix of radio systems to support command, control, communication and intelligence (C3I) functions. Due to high propagation losses and lack of covertness the capacities of these current systems are limited with respect to supporting the traffic loads of emerging multimedia C3I systems [1]. Thus there has been much interest for investigating new waveforms, protocols and networks that enhance throughput, data rates, efficient utilization of bandwidth, performance and covertness while maintaining operations in frequency bands where propagation characteristics are optimal for tactical operations. Modern operations take place in a highly mobile and volatile battlefield where multiple divisions spread out over a large area communicate with each other through a command structure [2]. Tactical wireless communication systems of the future are expected to support a variety of traffic (voice, video and data), interface seamlessly with landline communication systems and operate in a covert manner.

Military wireless communication systems must therefore be robust and survive at close

proximity to enemy territory under conditions of rapid change and equipment failures. The networks must be inherently adaptive to exist under dynamic conditions. They must be easily reconfigurable and capable of rapid deployment. Further, they must be resistant to interception and jitter being on the front lines of attack. Low Probability of Detection (LPD) and Low Probability of Intercept (LPI) are important characteristics for tactical military networks. LPD refers to the probability that an hostile interceptor can detect the presence of the communication signal and LPI refers to the probability of decoding and retrieving the transmitted information.

Distributed architectures are now being considered by the military for their resilience to regional attacks. Conventional narrow band CDMA was being used as the primary communication system in the military, but Ultra Wideband (UWB) systems with code division multiple access to spread the signal is being considered as a potential system for the future.

An ultra wideband system called Impulse Radio (IR) has been proposed in [3][4][5][6][7]. IR takes advantage of the available impulse signal technology in which the information carrying waveform is an extremely narrow pulse which has a bandwidth of 1 to 3 GHz. User separation and spectral smoothing are acheived by pseudorandom shifts.

Impulse Radio has been proposed as a candidate for future tactical networks for the following reasons. The communication pulses are baseband pulses and are dithered without the use of a carrier, thus obviating the need for removal of the carrier signal and hence making the system simpler. Multipath can be resolved to within a nanosecond in differential path delay thus eliminating multipath fading with proper signal processing. As a result, link budget margins to compensate for fading losses can be reduced. A well designed multiple-access impulse radio network could accommodate a large number of

users because of the significant bandwidth [4]. Multi-user interference is reduce because of the low duty cycle and occur only when pulses collide. Bit rates can be easily adjusted by changing the number of pulses per bit. Due to low power spectral density, IR has also been assumed to be more covert when compared to conventional CDMA systems.

Covert communication systems conduct information transfer in ways which lower the probability of unauthorized intercept and extraction of information about the message and about the transmitter. These systems employ coding schemes which are known only to the desired receiver and also spread the signal so that the observation bandwidth for the interceptor increases thereby making it more difficult to observe and decode the signal. The modulation schemes used spread the signal in a manner which is known only to the intended receiver which can then de-spread the signal and then decode the result to get the information. Impulse radio uses pulse position modulation with pseudo-random dithering to spread the signal. The duty cycle for impulse radio is very low making it difficult for an intercepting receiver to "tune" the signal without prior knowledge of the pulsewidth. Due to the gaps in the signaling scheme of impulse radio an intercepting receiver would have to process more noise energy and continuously vary its observation interval resulting in performance degradation [8].

Current Commercial Off-The-Shelf (COTS) systems are based on a centralized cellular architecture where basestations control direct communication between mobile users. This compromises survivability and and robustness because failure of the control center would disrupt communications. High transmit powers from the basestations due to location identification leave the network susceptible to jamming. The cellular architecture also suffers from increased time of deployment caused by the need for establishing a basestation infrastructure and relative rigidity in adapting the network to changing

battlefield conditions.

The advantages of impulse radio also result in design challenges [7]. The usage of nanosecond pulses and large bandwidth impose regulatory restrictions on transmitted power. The ultra-fine time resolution would require long synchronization times and perhaps require additional correlators and more signal processing at the receiver to capture sufficient signal energy.

Because of the disadvantages involved, it is essential to quantify the performance improvement over conventional cellular networks to evaluate the benefits of using impulse radio for military communications. The lack of an LPD waveform and covert signaling scheme is cited as one of the mains reasons against the use of COTS and for the use of impulse radio for military communications. However, beyond qualitative assertions there is rarely any quantitative evidence to evaluate the covertness of impulse radio. In this thesis we quantify the performance gain of impulse radio when compared with DS-CDMA and also evaluate the covertness of impulse radio by using a wideband radiometer as the intercepting receiver. The covertness can then be compared against conventional cellular systems to evaluate the gains achieved. In [9] a power control scheme and a peer to peer network topology is considered for impulse radio. In this work, we modify the power control scheme to remove saturated links and thus enhance covertness and also evaluate the covertness consistency of the peer-to-peer topology and suggest ways of modifying the topology to maintain covertness under different scenarios. This work has been undertaken in an attempt to address the design issues, the resolution of which would eventually result in the development of impulse radio as an effective, functional and flexible military wireless communication system.

1.2 Thesis Overview

1.2.1 Comparison with DS_CDMA

Impulse radio is an ultra wideband system which uses a time-hopping CDMA scheme with pulse position signaling. Pulse position signaling involves encoding binary digits by different shifts of the unmodulated signal. Carriers are not used to raise the signal to a frequency band but instead communication is achieved using a series of pulses of the order of a nanosecond in width [4]. An effective evaluation of the multiple access performance of this system can be acheived only by comparing it with a contemporary Direct sequence (DS) CDMA system tailored to be ultra wideband. Since communication in impulse radio is in the baseband an equivalent construction must be developed for DS CDMA for fair comparison. In Chapter 3, an unmodulated DS CDMA system model is considered which uses a sub-nanosecond sinusoidal pulse for transmission. The system characteristics and performance are similar to standard narrowband DS CDMA. The two systems: Impulse radio and the modified DS CDMA, are compared for multi-user environments, both in the presence and the absence of severe local interference. The results show that impulse radio performs better than DS CDMA and also quantify the performance gain achieved.

1.2.2 Covertness Quantification

Covertness can be defined as a measure of a wireless communications system's immunity to detection by an intercepting receiver. A quantitative evaluation of the covertness of impulse radio using a simple, sub-optimal radiometer detector under the assumption of Gaussian statistics was reported in [10]. This assumption is not applicable to impulse

radio due to the low duty cycle pulses.

In Chapter 4, we relax the Gaussian assumption to obtain a more accurate measure of the covertness of impulse radio. An objective is to quantify the worst-case covertness of impulse radio. To achieve this, we evaluate the covertness of impulse radio using a more complex "multi-radiometer" detection system ideally suited for detecting time-hopping, impulse radio signals, for single and multiple user cases. In addition to quantifying the worst-case covertness, we also investigate a number of other cases where the detector has varying amounts of prior knowledge of the transmitted, impulse radio signal. The covertness obtained for impulse radio is compared to more traditional wideband CDMA and narrowband CDMA (IS-95).

The pseudorandom signaling sequence of impulse radio is unknown to an intercepting receiver. We develop a multi-radiometer detection system that can be more sensitive to the low duty cycle, time-hopping impulse radio signal to challenge the covertness assertion. The multi-radiometer detection system can be viewed as a combination of time-contiguous, multiple wideband radiometers, with outputs that are OR'd together and the result compared to a threshold. The complexity of the multi-radiometer system makes closed-form analysis intractable, and thus we use simulation to evaluate covertness of impulse radio with a multi-radiometer detector.

The covertness of impulse radio is compared with that of conventional direct sequence Code Division Multiple Access (CDMA) schemes for which the covertness is calculated by well documented analytical expressions. Also considered are multiple user scenarios where the covertness is evaluated when multiple user pulses overlap as well as the case when the pulses are non-overlapping. The results show that impulse radio is considerably more covert than conventional DS-CDMA systems for all the cases considered.

1.2.3 Covertness of an IR Network Topology

Wireless network architectures can be broadly classified into centralized and distributed systems. Cellular systems conventionally follow the centralized system where the geographical area is divided into cells, each cell serviced by a basestation. The structure is essentially hierarchical wherein a group of basestations is controlled by a basestation switching center (BSC) and a group of BSC's controlled by a mobile switching center(MSC). The basestations perform intra-cellular functions like power control and routing of calls. The BSC handles handovers between basestations and channel assignment among other network functions. The functionality of the MSC includes the management of BSC's, inter-network compatibility and interfacing with landline networks. The survivability of such an architecture in hostile environments is poor because of the concentrated nature of control. The failure of a basestation results in isolation of the mobile users leaving the network vulnerable. The cellular architecture also suffers from increased deployment time due to basestation infrastructure and the rigidity of the topology in adapting to changing battlefield conditions.

Distributed packet radio architectures avoid the concentration of functionality into a control center. Distributed architectures have been proposed for packet radio networks in the literature [11][12][13][14]. The functionality is kept at the link level as much as possible with individual links monitoring the transmitter and receiver powers. The nature of packet radio architectures improves the survivability of the network and also allows for rapid deployment and reconfigurability.

A non hierarchical peer-to-peer topology with distributed power control has been proposed in [9]. We consider the links between mobile users to be sustained links where the connection is not terminated during silent periods and bit rate variations. In Chap-

ter 5, we extend the power control algorithm to eliminate saturated links by link level monitoring. Saturated links are links which do not attain the desired signal quality even though transmission is at maximum power levels. We observed that in a peer-to-peer topology the covertness degrades when the link lengths increase beyond an upper bound. We specify a suitable covertness value which is used as the covertness benchmark for a particular topology. The performance of impulse radio is evaluated and the optimum link length is quantified for a given set of parameters in order to maintain the specified covertness benchmark.

Chapter 2

Impulse Radio System Model

2.1 Physical Layer

The transmitted signal in impulse radio is constructed from a series of sub-nanosecond impulses which are shifted in time according to a distinct *time-hopping* code that is unique for every user [4][7][6]. Binary information is encoded by further shifting the pulses according to a pulse-position signaling scheme. The k^{th} transmitter's output signal $s^{(k)}(t)$ is given in [4] as

$$s^{(k)}(t) \;=\; \sum_{j=-\infty}^{\infty} w\left(t - jT_f - c_j^{(k)}T_c - d_j^{(k)}\right) \tag{2.1}$$

where t is the transmitter clock time, and $w(t)$ represents the transmitted monocycle waveform. The *frame time* T_f typically may be a hundred to a thousand times the monocycle width resulting in a signal with a very low duty cycle. The c_j's correspond to distinct pulse shifts in the time-hopping pattern specific to user k. The d_j's correspond to additional shifts to the pulse sequences to encode the binary data stream according to

the pulse-positioning scheme. In this modulation scheme a single symbol has a duration $T_s = N_s T_f$ where the number of monocycles N_s is determined by the bit rate.

When N_u users are active in the system, the received signal $r(t)$ can be modeled [4] as

$$r(t) \;=\; \sum_{k=1}^{N_u} A_k s^{(k)}(t - \tau_k) + n(t) \tag{2.2}$$

where A_k models the attenuation of the signal over the channel and τ_k represents the timing mismatch between the transmitter and the receiver for the user k. Under the assumption that the interfering signals have the same power level as that of the desired user, and the time offsets of interfering pulses arriving at the receiver are independent and uniformly distributed random variables over the frame time $[0, T_f)$, the total interference can be modeled as a Gaussian random process [4]. The interference also can be considered to be zero mean because the pulse shape selected for impulse radio: the Gaussian monopulse integrates to zero and hence the average of the total interference at the output of the receiver is zero. The probability of error is given in [4] as

$$P_{error}(N_u) \;=\; \frac{1}{\sqrt{2\pi}} \int_{\sqrt{SNR(N_u)}}^{\infty} exp\left(\frac{-x^2}{2}\right) dx \tag{2.3}$$

where the $SNR(N_u)$ is the output signal to noise ratio for a particular number of users N_u and is given in [4] as

$$SNR(N_u) \;=\; \frac{1}{\frac{\sigma_n^2}{(A_1 N_s m_p)^2} + \frac{1}{N_s}\frac{\sigma_a^2}{m_p}\sum_{k=2}^{N_u}\left(\frac{A_k}{A_1}\right)^2} \tag{2.4}$$

where m_p is the receiver correlator output for a single received pulse, σ_a^2 is the variance of the interfering users, σ_n^2 is the thermal noise power or variance, and A_k models the

attenuation of the signal from the k^{th} user. A_1 is the required amplitude for the signal of the desired user to meet the performance criteria specified in terms of the probability of error in the single user case. The equation for the probability of error in the single user case is given in [4] as

$$SNR(N_1) = \frac{(A_1 N_s m_p)^2}{\sigma_n^2} \tag{2.5}$$

Chapter 3

Performance Comparison with DS-CDMA

3.1 Introduction

Ultra-wideband communication systems use signals that occupy extremely large bandwidth. The signal is therefore more covert because of lower power density and has higher immunity to the effects of multiple access interference. Rayleigh fading ceases to be a significant bottleneck due to multipath immunity because of the high resolution capabilities of the receiver [6][15][16]. Thus, ultra-wideband systems evince great potential for future tactical radio networks.

Impulse radio does not use sinusoidal carriers to raise the signal to a frequency band but instead communicates using a series of pulses of the order of a nanosecond in width [4]. An effective evaluation of the multiple access performance of this system can be done only by comparing it with a contemporary Direct sequence(DS) CDMA system tailored to be adequately ultra wideband. In this report, an unmodulated DS CDMA system

model is considered which used a sub-nanosecond sinusoidal pulse for transmission. The system characteristics and performance are similar to standard narrowband DS CDMA. The two systems: Impulse radio and the modified DS CDMA, are compared for multi user environments, both in the presence and the absence of severe local interference.

3.2 Direct Sequence CDMA

Cellular radio systems are essentially narrowband systems employing rectangular pulses modulated by a sinusoidal carrier. For effective comparison of the ultra wideband impulse radio system with DS-CDMA, the cellular radio system is modeled as a wideband system.

System Model

We consider the direct sequence equivalent of the Gaussian monopulse to be a simple sinusoidal pulse having the same frequency as the monopulse. Thus, the time period of the sinusoidal pulse is of the order of one nanosecond. The frequency spectra then becomes large enough for effective comparison. A comparison of the spectra of the pulses of the two systems is shown in figure 3.1.

Direct Sequence calls for continuous transmission of chips which make up a bit. We consider a *single* sinusoidal pulse to be equivalent to one chip. This is a variation from standard DS CDMA where there are a number of carrier pulses per chip [17]. This condition is imposed to ensure that the system becomes wideband while still maintaining the basic characteristics of the DS CDMA system. Thus the total number of chips in our system model would be the total number of time slots, each time slot equal to one chip width, in one bit in the impulse radio system. This then means that the number of chips in our model would be much larger than the number of chips in impulse radio as the

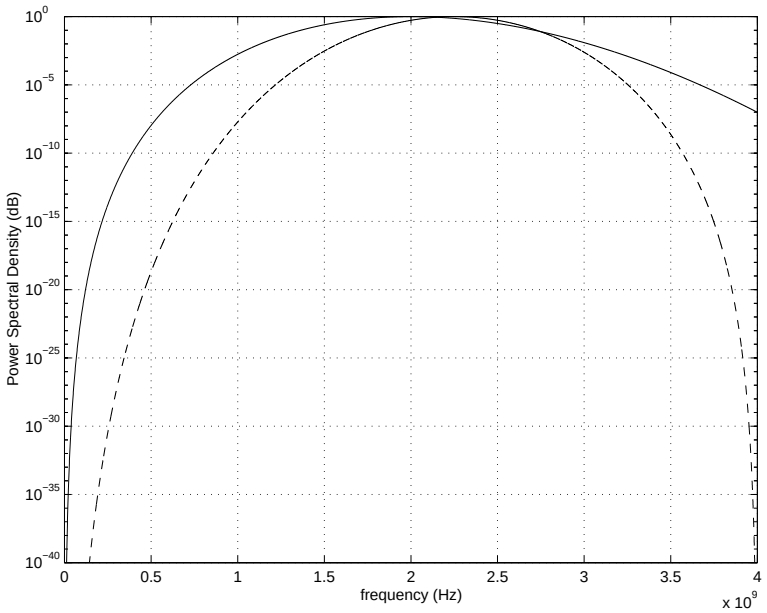

Figure 3.1: Plot of the spectra for the Gaussian monopulse and the sinusoidal waveform.

latter has only one pulse per frame per bit [4]. Consequently, for the same transmitted power, the amplitude of the pulse in the DS CDMA model would decrease. The power for Impulse radio is given by $P_i = A_i^2 m_p N_s T_b^{-1}$, [4] and that of the DS CDMA model is $P_c = A_c^2/2$ [18]. Equating both powers and noting that since the bit rate is the same $T_b = N_c T_c$ where N_c is the number of chips in the DS CDMA model, we have

$$A_c \;=\; \sqrt{\frac{2\,A_i^2\,m_p N_s}{T_c N_c}} \tag{3.1}$$

Since N_c is much greater than N_s, the amplitude of the CDMA system A_c is smaller than that of the equivalent impulse radio system A_i to compensate for the much higher duty cycle.

In the case of perfect power control where all the interfering users have the same power level as the desired user, we can make the Gaussian assumption for the Multiple

Access Interference for asynchronous detection. We can then use the result given in [18] for the probability of error,

$$P_e \;=\; Q\left(\sqrt{\frac{1}{\frac{K-1}{3\,N} \;+\; \frac{N_o}{2T_bP_o}}}\right) \tag{3.2}$$

where P_e is the probability of error, K is the number of users, N is the number of chips per bit, N_o is the noise power spectral density, T_b is the time duration of a single bit and P_o is the power in Watts.

The Gaussian assumption is also made in impulse radio and since the monopulse is not modulated by a carrier, the noise is considered to be baseband or lowpass [4]. For effective comparison and since the sinusoidal pulse is of the same width as the monopulse, the noise in the DS CDMA model is also considered to be baseband. The signal power is selected so as to obtain a single user probability of error of 10^{-3} in the noise-limiting case and is the same as that used in the impulse radio communication system.

The performances of both the impulse radio system and the modified DS CDMA system were compared for perfect power control as the number of users increase. The results are given in the next section.

Near-Far effect

The network topology considered contains large local interferers as well as distant interferers [9]. Thus it becomes important to investigate the performance of the system for unequal power levels of the interfering users and the desired user. In particular we consider three local interferers and then compare the probability of error for both the impulse radio and DS-CDMA when the power levels of the local interferers are varied.

Ideally, in the network architecture specified above, the power control algorithm given in [9] increases the power level of the desired user if and when the power levels of any local interferers increase. But, for the purpose of evaluating the system performance, the power level of the desired user is assumed to be constant.

We use the Simplified Expression for the Improved Gaussian Approximation for evaluating the probability of error as it provides a more accurate evaluation of the CDMA model [19]. Defining ψ as the variance of the multiple access interference, the mean and the variance of ψ for the case of unequal power levels of the interfering users is given in [18][17] as

$$\mu_\psi = \frac{NT_c^2}{6} \sum_{k=1}^{K-1} P_k$$

$$\sigma_\psi^2 = \frac{T_c^4}{4} \left[\left(\frac{23N^2 + 18N - 18}{360} \sum_{k=1}^{K-1} P_k^2 \right) + \left(\frac{N-1}{36} \sum_{k=1}^{K-1} \sum_{j=1, j\neq k}^{K-1} P_k P_j \right) \right]$$

The probability of error is then given in [18][17] as (for the case when the noise term is significant)

$$\begin{aligned} P_e &\approx \frac{2}{3} Q \left(\sqrt{\frac{P_o T_b^2}{2\left(\mu_\psi + \frac{N_o T_b}{4}\right)}} \right) \\ &+ \frac{1}{6} Q \left(\sqrt{\frac{P_o T_b^2}{2\left(\mu_\psi + \sqrt{3}\sigma_\psi + \frac{N_o T_b}{4}\right)}} \right) + \frac{1}{6} Q \left(\sqrt{\frac{P_o T_b^2}{2\left(\mu_\psi - \sqrt{3}\sigma_\psi + \frac{N_o T_b}{4}\right)}} \right) \end{aligned}$$

where μ_ψ and σ_ψ are defined earlier and P_o, T_b and N_o represent the power, bit length and noise power spectral density respectively.

Since, the power levels of the interfering users, though different, are assumed to be constant, the Simplified Expression for the Improved Gaussian approximation does not provide results much different from those provided by the Standard Gaussian Approximation. The equation used in that case would be [18]

$$P_e \;=\; Q\left(\sqrt{\frac{1}{\frac{1}{3N}\sum_{k=1}^{K-1}\frac{P_k}{P_o} \;+\; \frac{N_o}{2T_bP_o}}}\right)$$

We compare the impulse radio system versus the DS CDMA was done for three local interferers in terms of the probability of error as the number of users increases. The results are presented in the next section.

3.3 Simulation parameters and plots

We assume that all the users are stationary. The effect of Rayleigh fading is neglected in view of the large system bandwidth.

The single user SNR is set to 9.55 dB, corresponding to a single user error probability of 10^{-3}. For $f_c = 2$ GHz, $T_f = 100$ ns and $\delta = 0.194 \times 10^{-9}$ s, we use the equations given in [4] to obtain $m_p = 2.7724 \times 10^{-10}$, $\sigma_a^2 = 1.7467 \times 10^{-22}$ and $\sigma_n^2 = 1.14832 \times 10^{-30} \times N_s$. The probability of error for impulse radio is calculated using equations 2.3 and 2.4.

Section 3.2 compares the performance of the impulse radio system and modified version of DS CDMA in terms of the probability of error both in the presence and the absence of severe local interference.

Figure 3.2 shows the performance comparison of both the impulse radio system and the DS CDMA system in terms of the probability of error as the number of users increase.

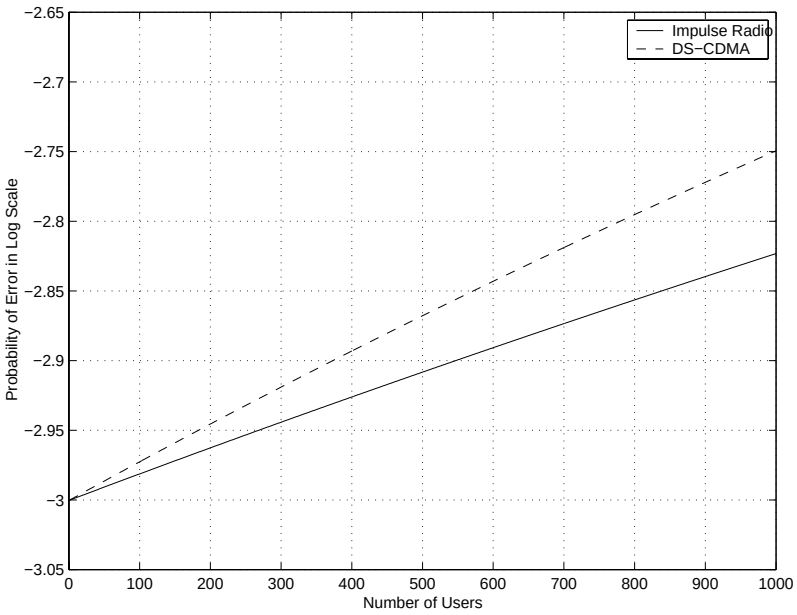

Figure 3.2: Plot of the probability of error as a function of the number of users for both the impulse radio system and DS CDMA system.

The power level of all the users (desired as well as interfering) are assumed to be the same and constant and the detection is considered to be asynchronous. It can be seen that impulse radio performs better than the DS CDMA system through the entire range of the number of users, the difference becoming more significant for a large number of users.

Figures 3.3 and 3.4 shows the variation of the probability of error with bit rate while keeping the total number of users and the total number of chips per bit a constant. It is clear that impulse radio has a lower probability of error for the entire range of bit rates.

Figure 3.5 shows the variation of bit rate versus the number of users for a constant probability of error. Assuming constant probability of error and constant bit rate, it can be seen that impulse radio supports a larger number of users.

Figure 3.6 compares the performances of impulse radio and the DS CDMA system for

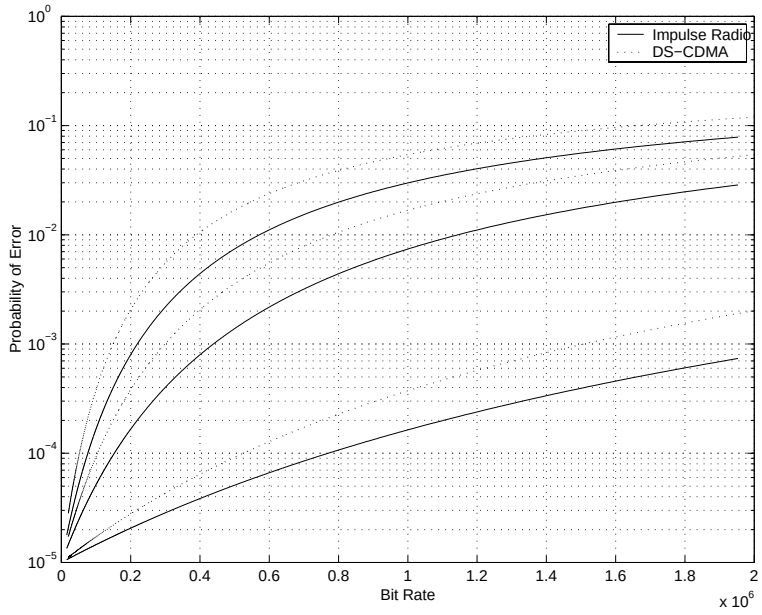

Figure 3.3: Plot of the probability of error versus bit rate for both the impulse radio system and the DS CDMA system.

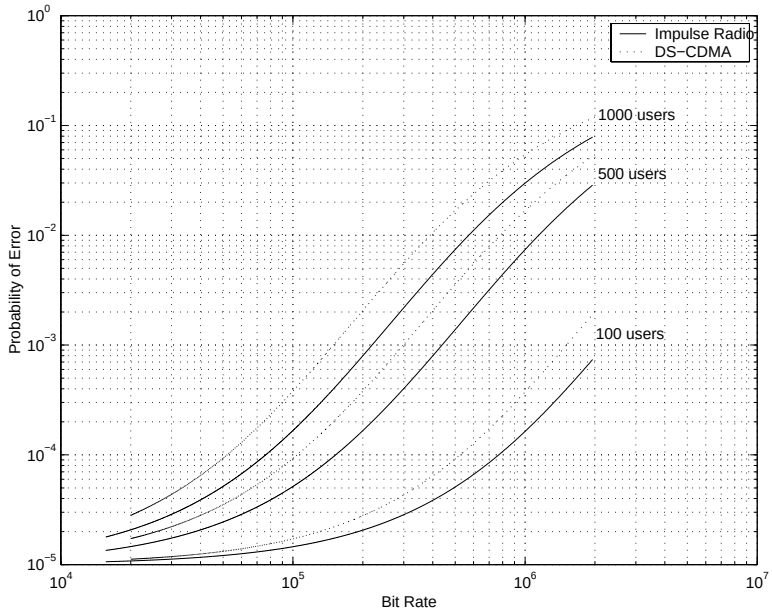

Figure 3.4: Plot of the probability of error versus bit rate for both the impulse radio system and the DS CDMA system.

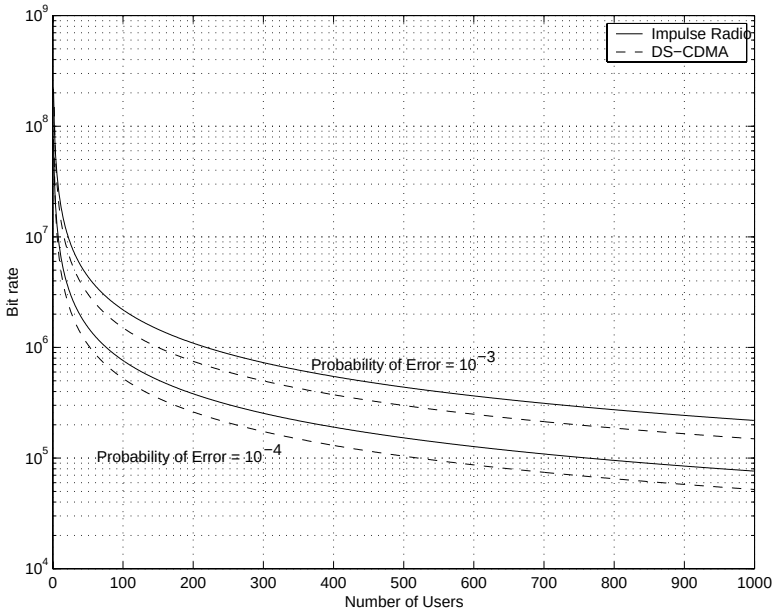

Figure 3.5: Plot of the bit rate versus the number of users for a constant probability of error for both the impulse radio system and the DS CDMA system.

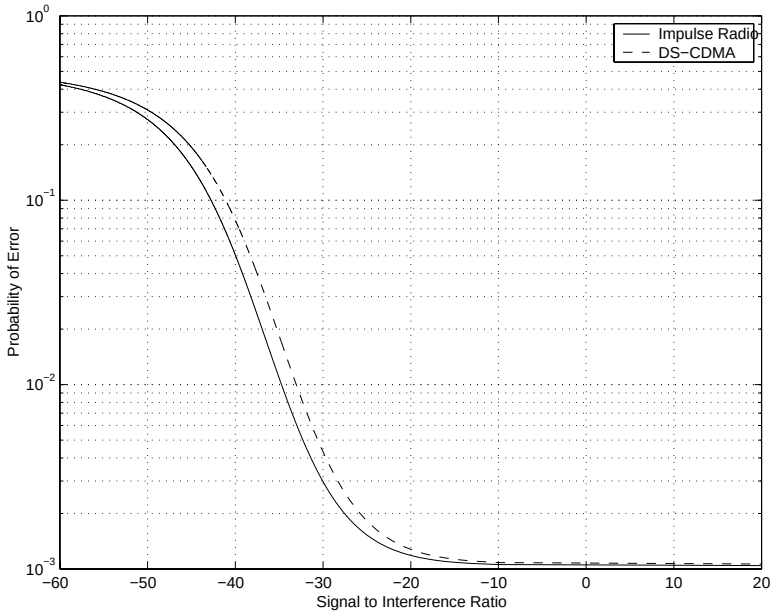

Figure 3.6: Plot of the probability of error as a function of the signal to interference ratio for three local interferers for both the impulse radio system and the DS CDMA system.

three local interferers. The power levels of all the other interfering users are considered to be the same as that of the desired user. Clearly, impulse radio performs better than the DS CDMA system for all power levels of the interfering users.

Chapter 4

Quantifying Covertness of Impulse Radio

4.1 Introduction

Covertness can be defined as a measure of a wireless communications system's immunity to detection by an intercepting receiver. Covert operation, i.e., systems exhibiting low probability of detection (LPD), is highly desirable for tactical communications systems. In spite of the importance of covertness for tactical communications systems, only qualitative assertions are typically made regarding the relative covertness of one communications system to another. Impulse radio is an ultra-wideband communication system which has features, one of which is good covertness, that make it a promising candidate for tactical military communications. A quantitative evaluation of the covertness of impulse radio using a simple, sub-optimal radiometer detector under the assumption of Gaussian statistics was reported in [10]. This assumption is not applicable to impulse radio due to the low duty cycle pulses.

We relax the Gaussian assumption to obtain a more accurate measure of the covertness of impulse radio. An objective is to quantify the worst-case covertness of impulse radio. To achieve this, we evaluate the covertness of impulse radio using a more complex "multi-radiometer" detection system ideally suited for detecting time-hopping, impulse radio signals, for single and multiple user cases. In addition to quantifying the worst-case covertness, we also investigate a number of other cases where the detector has varying amounts of prior knowledge of the transmitted, impulse radio signal. The covertness obtained for impulse radio is compared to more traditional wideband CDMA and narrowband CDMA (IS-95).

The most widely used system for the detecting receiver is the well-known wideband radiometer [20]. The measure used most often to quantify covertness is the signal power-to-noise density ratio S/N_0 required to meet a desired set of performance indices specified for the detecting receiver. The performance indices of the detecting receiver are typically specified in terms of the probability of signal detection P_d and the probability of false alarm P_{fa}. A solution for S/N_0 to meet the desired performance criteria is not available in closed form, but there have been a number of models proposed which simplify the analysis of the wideband radiometer and provide the required S/N_0 under certain assumptions which are not all applicable to impulse radio.

The impulse radio signaling scheme uses a time-hopping CDMA with pulse position signaling. The pulse shape employed is the Gaussian monocycle. The pseudorandom sequence is unknown to the radiometer detection receiver. We develop a multi-radiometer detection system that can be more sensitive to the low duty cycle, time-hopping impulse radio signal. The Gaussian assumption is not used since it does not apply. The multi-radiometer detection system can be viewed as a combination of time-contiguous, multiple

wideband radiometers, with outputs that are OR'd together and the result compared to a threshold. The impulse radio signal does not satisfy the assumptions required by the radiometer models. In addition, the complexity of the multi-radiometer system further complicates closed-form analysis, and thus we use simulation to evaluate covertness of impulse radio with a multi-radiometer detector.

In Section 4.2.1 we introduce the wideband radiometer and analytical models and present the multi-radiometer detector. The multi-radiometer detector with appropriate prior knowledge represents the best detector for time-hopping impulse radio signals. In Section 4.3, the covertness is evaluated for the single user case, where the detector has varying amounts of prior knowledge about the impulse radio signal. The multiple-user case is considered in Section 4.4 for both overlapping and non-overlapping pulse configurations.

The simulation setup and results are presented in Section 4.5. The covertness is determined for the optimal single user case, when the detector has complete knowledge about the bandwidth and the pulse width of the system, as well as the sub-optimal single user case when the detector has little prior knowledge about the impulse radio system specifications. In addition, the covertness of impulse radio is compared with that of conventional direct sequence Code Division Multiple Access (CDMA) schemes for which the covertness is calculated by well documented analytical expressions. Also considered are multiple user scenarios where the covertness is evaluated when multiple user pulses overlap as well as the case when the pulses are non-overlapping. Finally, the "average covertness" of impulse radio for a specified number of users is determined and then compared to DS-CDMA schemes with equivalent number of users. The results show that impulse radio is considerably more covert than conventional DS-CDMA systems for

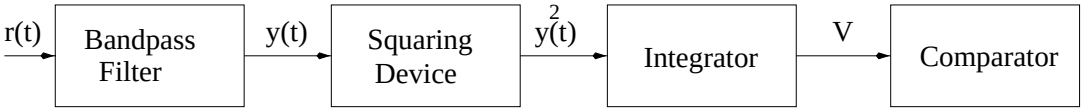

Figure 4.1: Radiometer block diagram.

all the cases considered.

4.2 Radiometer Detectors

The fundamental component of most detection receivers is the radiometer. This section describes the wideband radiometer detector, and presents the multi-radiometer detector.

4.2.1 Wideband Radiometer

The optimal receiver for detection of a signal in white Gaussian noise is the *energy detector* or the *radiometer*. It is easily implemented in hardware and can be used to detect spread spectrum signals [8]. A block diagram of the radiometer is shown in Figure 4.1.

Detection is accomplished by calculating the energy of the received message and comparing with a predetermined threshold. The wideband radiometer uses a single channel of a particular bandwidth to calculate energy over an observation interval. It consists of a bandpass filter of bandwidth W, a squaring device and an integrator with an integration time T set equal to the observation time interval. The alarm circuitry implements a simple thresholding system.

The received signal is input to the filter followed by the squaring device and the T-second integrator. The output of the integrator is fed to a comparator with a fixed threshold level. If the integrator output is higher than the threshold, then the signal

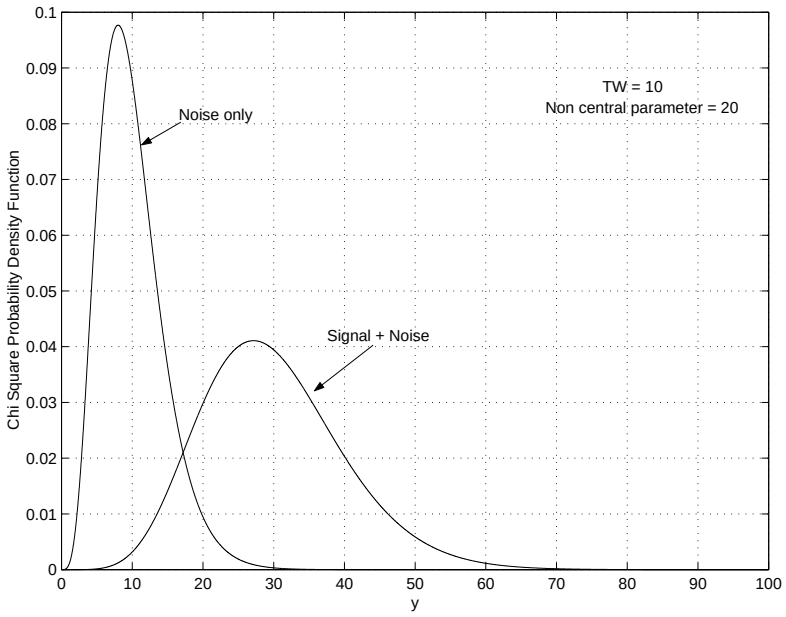

Figure 4.2: Chi-square distributions for $TW = 10$ and $\lambda = 13$ dB.

is declared present. The performance of the radiometer is generally characterized by the probability of detection P_d (signal and noise present), the probability of false alarm P_{fa}(noise only) and the Signal power-to-Noise power spectral density S/N_0 which is a measure of the required signal power to achieve the target P_d and P_{fa} values.

The threshold V_t of the radiometer is selected to meet the P_{fa} criterion such that the radiometer generates a false alarm when there is no signal present with probability P_{fa}. Then the S/N_0 is determined for a given P_d. Thus the required S/N_0 can be considered as a measure of covertness of the communication system of interest.

When the signal is absent and the input to the radiometer is strictly additive white Gaussian noise with two-sided power spectral density $N_o/2$ and the statistics of the output of the radiometer V are normalized, then the normalized random variable $Y = 2V/N_o$ has a central chi-square distribution with $\upsilon = 2TW$ degrees of freedom where T and W are the observation time interval and the filter bandwidth of the radiometer respectively.

The probability density of Y is given by [20]:

$$p_n(y) = \frac{1}{2^{\upsilon/2}\Gamma\left(\frac{\upsilon}{2}\right)} y^{(\upsilon-2)/2} e^{-y/2}, \qquad y \geq 0 \tag{4.1}$$

When the signal is present at the input to the radiometer with energy E measured over time T, then the random variable Y has a non-central chi-square distribution with $2TW$ degrees of freedom and non-central parameter $\lambda = 2E/N_o$. The probability density of Y can then be written as [20]:

$$p_{sn}(y) = \frac{1}{2}\left(\frac{y}{2}\right)^{(\upsilon-2/4)} e^{-(y+\lambda)/2} I_{(\upsilon-2)/2}\left(\sqrt{y\lambda}\right), \quad y \geq 0 \tag{4.2}$$

where $I_n(z)$ is the nth order modified Bessel function of the first kind. Examples of these densities are shown in Figure 4.2 where $TW = 10$ and $\lambda = 20$ $(E/N_o) = 10$ dB. The P_{fa} and the P_d values of the radiometer can now be determined by integrating the respective conditional densities as shown:

$$P_{fa} = \int_{2V_T/N_0}^{\infty} p_n(y)dy \tag{4.3}$$

$$P_d = \int_{2V_T/N_0}^{\infty} p_{sn}(y)dy \tag{4.4}$$

where V_T is the alarm threshold of the radiometer against which the output of the radiometer is compared.

The threshold V_T and the S/N_0 are determined in order to satisfy the performance criteria of the radiometer, described by P_{fa} and P_d in (4.3). However, the equations in (4.3) cannot be solved in closed form and must be evaluated numerically. Several

radiometer models have been developed by approximations and detection curves based on numerical results. The simplest of these models is the Edell's model [20] which is applicable in cases when the number of degrees of freedom (i.e., the time-bandwidth product) is very large. When TW becomes large, the chi-square and the non central chi-square density functions asymptotically converge to a Gaussian by the central limit theorem. Gaussian output statistics from the radiometer can then be assumed which greatly simplifies analytical calculations. The signal-to-noise density ratio for a given radiometer performance described in terms of P_{fa} and P_d is then given by [21]:

$$\left(\frac{S}{N_0}\right)_{req} = d\sqrt{\frac{W}{T}} \tag{4.5}$$

where W and T are the bandwidth and the observation interval of the radiometer and $d = \left[Q^{-1}\left(P_{fa}\right) - Q^{-1}\left(P_d\right)\right]$. When TW is small, as in the case of impulse radio, an error is introduced in making the Gaussian assumption. A correction factor η is thus introduced to account for the error. The S/N_0 then becomes

$$\left(\frac{S}{N_0}\right)_{req} = \eta d\sqrt{\frac{W}{T}} \tag{4.6}$$

In Edell's model the correction factor is selected from curves obtained by numerical results. Other radiometer models provide expressions for the correction factor. The Park's model is suitable for all ranges of TW and gives the correction factor η as

$$\eta = \frac{1}{4}\sqrt{\frac{d^2}{TW}}\left(\sqrt{1 + 18.4\frac{TW}{d^2}}\right) \tag{4.7}$$

Thus, the Park and the Edell models are similar in form but the correction factor is no longer needed for small TW products. The Park's model can be expressed as [20]:

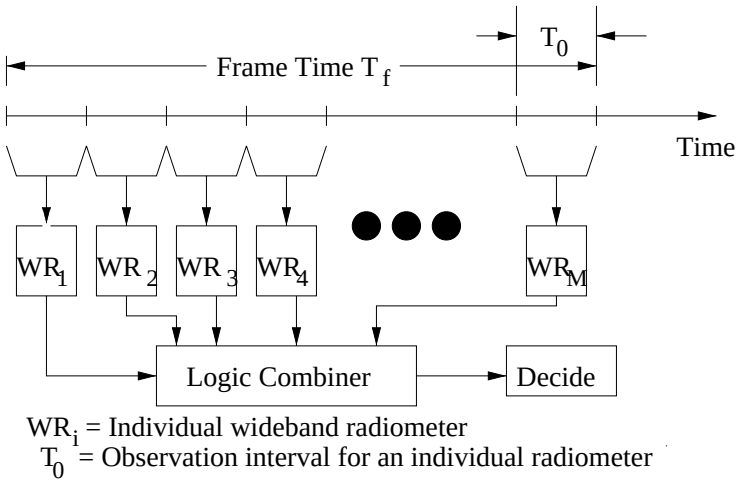

Figure 4.3: Multi-radiometer system used to detect impulse radio signals.

$$\left(\frac{S}{N_0}\right)_{req} = \frac{X_0 + \sqrt{X_0^2 + 18.4TWX_0}}{4T} \tag{4.8}$$

This model can be used for all TW products for a signal in white Gaussian noise. However, the optimum intercepting receiver in the impulse radio communication system has a different radiometer setup because of the signaling scheme used in impulse radio. We show in the sequel that some of the assumptions required to obtain the expression for S/N_0 are also not valid in impulse radio. As a result, we use simulation to accurately determine the signal power-to-noise density ratio which is the criterion for covertness used in this thesis.

4.2.2 Multi-Radiometer System

The Gaussian monocycle pulse in impulse radio is pseudorandomly positioned within a frame time interval. So, the detector must be turned "on" for the entire frame interval. However, rather than generating one observation per frame, the frame time is covered by

M contiguous intervals of length T. Each of the M decisions is input to a logic combiner consisting of an "OR" circuit. Detection of a pulse by this multi-radiometer system is based on the output of this "OR" circuit.

An alternative way to view the multi-radiometer detector is shown in Figure 4.3. The entire time frame T_f is divided into M segments, the duration of each segment is the observation interval of an individual radiometer, T_o. Thus the M decisions generated by the M radiometers are input to the logic combiner. If any of the input decisions from the individual radiometers is positive, then the signal is declared to be present by the multi-radiometer system. It is possible to implement this circuit using a single radiometer and appropriate sample and hold circuitry.

We calculate the covertness of impulse radio using this multi-radiometer system where the amount of prior knowledge the intercepting receiver has about the impulse radio system is varied from case to case. The most sensitive detector is a multi-radiometer system that is perfectly synchronized with the received pulse with prior knowledge of pulse width as well as the bandwidth of the received signal. For this case the bandwidth of the input filters of the individual radiometers are set to the signal bandwidth and the observation intervals to the signal pulse width. For systems with less sensitivity the parameters of the multi-radiometer system are adjusted according to known parameters of the system.

4.3 Single User Scenario

The performance (i.e., the probability of detection P_d and the probability of false alarm P_{fa}) of the entire radiometer system is a function of the performance (P_{di} and the P_{fai}) of the individual radiometers. The analytical models (Park's and Edell's) assume that only

one radiometer with a single observation and integration interval is used for detection. The models also assume that there is significant signal energy present for the entire duration of the observation interval. But impulse radio signals consist of low duty cycle Gaussian monocycles, thus if the observation interval of the individual radiometers is increased beyond the pulse width then the signal is limited to only part of the observation interval and additive while Gaussian noise makes up the rest. Furthermore, the Gaussian assumption for the output statistics of the radiometer is invalid because impulse radio is an ultra-wideband communication system with $TW \approx 1$. For these reasons, theoretical models are not applicable and hence we use simulation to quantify the covertness of impulse radio.

Since the individual radiometers within a frame have identical characteristics, the probability of false alarm P_{fai} and the probability of detection P_{di} are the same. The P_{fa} and the P_d for the entire multi-radiometer system can be expressed in terms of the P_{fai} and P_{di} of the individual radiometers as:

$$P_d = \left[1 - \left\{(1 - P_{di})\ (1 - P_{fa})^{M-1}\right\}\right] \tag{4.9}$$

$$P_{fa} = \left[1 - (1 - P_{fai})^M\right] \tag{4.10}$$

This is valid for the single user case when there is a single pulse to be detected within a frame and M radiometers within a frame.

Given P_{fa} and P_d for the multi-radiometer system, the individual P_{fai} and P_{di} can be calculated iteratively. The threshold for the individual radiometers is determined by simulation to meet the P_{fai} criterion and then, given this threshold value, the S/N_0 is found so as to meet the required P_{di} criterion.

The S/N_0 for wideband CDMA can be obtained from the theoretical models since the constraints which render the models inapplicable in impulse radio do not exist in wideband CDMA.

Since the bandwidth or the pulse width may not be known to the intercepting receiver, we consider the performance of the naive receiver, unaware of the system specifications. The system setup for the less sensitive receiver is similar in structure to the most sensitive or the optimal receiver but the observation interval or the bandwidth of the input filter may not be equal to the actual pulse width or the bandwidth of the impulse radio system. We consider the performance when the bandwidth is unknown but the pulse width is known and also the case when the pulse width is unknown but the bandwidth is known. However, perfect synchronization is assumed for the naive intercepting receiver as well. These scenarios are now considered in more detail.

4.3.1 Bandwidth Unknown

We consider the case when the impulse radio bandwidth is unknown. For this case, the receiver structure is similar to the optimal receiver with the same number of radiometers, M, and the observation interval set equal to the pulse width. However, if the bandwidth of the input filter of the radiometer is greater than the system bandwidth, then the noise power input to the square law detector and the integrator from the filter increases, and if the bandwidth is less than the system bandwidth the signal power input to the square law detector decreases.

4.3.2 Pulse Width Unknown

We assume in this case that the observation interval of the receiver is different from the actual pulse width of the Gaussian monocycle of impulse radio while the bandwidth is equivalent to the system bandwidth and is constant. If the observation interval is longer than the pulse width then more noise is input to the squaring device and the integrator. If the observation interval is smaller than the pulse width then portion of the signal is cutoff as well. Since the observation interval is different, the number of individual radiometers required to cover a frame as a function of the observation interval T_0. If we consider the observation interval of the naive receiver to be T_R, then the total number of radiometers in a frame is $M^{'} = T_f/T_R \neq M$ if $T_R \neq T_p$ where T_f is the length of one frame time and T_p is the pulse width of the Gaussian monocycle. The performance of the individual radiometers P_{fai} and P_{di} are then related to the system performance through $M^{'}$ as

$$P_d = \left[1 - \left\{(1 - P_{di})\ (1 - P_{fa})^{M^{'}-1}\right\}\right] \tag{4.11}$$

$$P_{fa} = \left[1 - (1 - P_{fai})^{M^{'}}\right] \tag{4.12}$$

The intercepting receiver which is unaware of both the system bandwidth and the pulse width of the Gaussian monocycle is not considered because of our objective to calculate covertness under optimal intercepting receiver conditions so as to obtain a quantitative covertness bound.

We have assumed the received signal to be perfectly time synchronized with the observation intervals of the individual radiometers for all the cases considered above.

For asynchronous signals, there is overlap into adjacent radiometer integration intervals. In the worst-case scenario, exactly half the signal overlaps onto the observation interval of the adjacent radiometer, since the radiometers are aligned in time, hence minimizing signal power in both radiometers. In this case, the signal power input to a particular radiometer is reduced by 3 dB. As a result the required S/N_0 to meet performance criteria and hence the covertness increases by 3 dB-Hz. The actual covertness of impulse radio at any point in time depends on the amount of signal overlap. Assuming that the covertness (S/N_0) under ideal time synchronization for a single user is C, then the actual covertness can be written as $C + \alpha 3$ dB-Hz where $0 < \alpha < 1$. However since our objective is to obtain an upper bound on signal detectability or a lower bound on covertness, the assumption of perfect synchronism is plausible.

4.4 Multiple-User Scenario

When multiple users are active in the network, the number of pulses in a particular time frame increases correspondingly. If k users are active, then there are k Gaussian monocycles which are pseudorandomly shifted within a time frame. The multi-radiometer receiver structure in this case remains the same but because of the presence of more pulses in the system and thus more energy per frame time, the performance of the individual radiometers (P_d) can be decreased, yet meeting the system performance criteria. The k pulses may or may not overlap with each other and as a result two cases arise. We assume that all that the monocycles have equal amplitudes. We also assume that the intercepting receiver has all the information about the system i.e., the bandwidth and the pulse width of impulse radio.

4.4.1 Non-Overlapping Case

In this case, we assume that the pulses occupy different time slots within a frame i.e., are non-overlapping. The multi-radiometer system for this case is similar to that in the single user case, except that relationship between the overall detector performance and the probability of detection P_{di} of the individual radiometers is a function of the number of users For k users in the system, the P_d of the overall system is related to the individual P_{di} by:

$$P_d = \left[1 - \left\{(1 - P_{di})^k \ (1 - P_{fai})^{M-k}\right\}\right] \tag{4.13}$$

The P_{fa} values of the radiometers remain unaffected by the number of users. Given the performance criteria for the individual radiometers, simulation is used to obtain the S/N_0 required for a specific value of P_{di}. The results are presented in section 6.

4.4.2 Overlapping Case

If k users are active in the system and x users overlap ($2 \leq x \leq k$), then amplitude increases by a factor of x and the probability of detection for the individual radiometers is given by (assuming complete overlap)

$$\begin{aligned} P_d &= \left[1 - \left\{(1 - P_{di})^{k-x+1} \ (1 - P_{fai})^{M-(k-x+1)}\right\}\right] \quad \text{for } k < M \\ &= \left[1 - \left\{(1 - P_{di})^{\left[\frac{M}{k}(k-x)+1\right]} \ (1 - P_{fai})^{M-\left[\frac{M}{k}(k-x)+1\right]}\right\}\right] \quad \text{for } k > M \text{ and } x > \frac{k}{M} \end{aligned} \tag{4.14}$$

$$= \left[1-(1-P_{di})^M\right] \text{ for } k > M \text{ and } x < \frac{k}{M}$$

Since we seek an upper bound on signal detectability, we assume complete overlap of the pulses.

The covertness is dependent on the number of overlapping pulses x, which varies between $2 \leq x \leq k$ from frame to frame depending on the pseudorandom positioning of the pulses from different users. To obtain a quantitative measure of covertness, we define the *average covertness* for a given number of users k as

$$C_k = \sum_{x=2}^{k} SNR_x \, p(x) \tag{4.15}$$

where C_k is the covertness value for k users and SNR_x is the signal-to-noise density ratio S/N_0 when k users are active and x pulses overlap and $p(x)$ is the probability that x pulses out of k pulses overlap. The P_{di} corresponding to this covertness value is given in (4.14).

We use simulation to evaluate (4.15) since this expression is intractable. Assuming that k users are active in the system, then each time frame has exactly k pulses which are pseudorandomly shifted within the frame. Since the probability that a pulse occupies a particular time slot in the frame is the same for all time slots, the individual user pulses are considered to be uniformly shifted within the frame. The maximum overlap for each frame can then be determined by randomly distributing the k pulses among the timeslots within the frame. Since the covertness for a particular frame only depends on the maximum overlap, the corresponding S/N_0 for that frame can be found. The

average covertness for a given number of users can be calculated by averaging the S/N_0 over the number of frames, where the maximum overlap for each frame is the maximum number of users which overlap in a single timeslot in the frame. The average covertness is also compared with wideband CDMA and IS-95. The covertness for CDMA systems are calculated by the analytical expressions given above with allowances made for multiple users resulting in decrease in covertness according to:

$$\left(\frac{S}{N_0}\right)_k = \left(\frac{S}{N_0}\right)_1 - 10\log k \tag{4.16}$$

The results are presented in the next section.

4.5 Simulation Setup and Results

The simulation of the radiometers was performed using Monte Carlo techniques. The users are assumed to be stationary for the duration of the simulation in the peer-to-peer network topology. Perfect power control is also assumed, which implies that all the pulses at the multi-radiometer detection system have equal amplitudes.

The impulse radio system uses a Gaussian monocycle of center frequency $f_c = 2$ GHz and pulse width $T_p = 6 \times 10^{-10}$ s. The frame time is $T_f = 6 \times 10^{-8}$ s. The number of timeslots in one frame time interval is $M = 100$. The bandwidth of the pulse is taken to be $B = 4$ GHz.

Table 4.1: Single user covertness values for impulse radio, wideband CDMA and IS-95.

System	Required S/N_0
Impulse radio	107.78 dB-Hz
Wideband CDMA	75.12 dB-Hz
IS-95	70.11 dB-Hz

4.5.1 Optimal Multi-Radiometer System Simulation

In the ideal case, the multi-radiometer system is assumed to have complete knowledge of the system specifications, i.e., the bandwidth and the pulse width. The performance criteria for the radiometer is assumed to be $P_d = 0.9$ and $P_{fa} = 1 \times 10^{-2}$. The input filter to an individual radiometer is implemented as a fourth order butterworth filter with a 4 GHz cutoff. The observation interval of the radiometer is T_p or the pulse width. To ensure simulation accuracy, signals are oversampled at a frequency of $f_s = 1.25 \times 10^{11}$ Hz.

The P_{fai} and the P_{di} values for the individual radiometers are calculated iteratively for the single user case using the equations given in (4.9). Additive white Gaussian noise is input to the radiometer and is sampled and filtered. The integrator is reset periodically after each observation interval T_p. The resulting signal is compared to a threshold to calculate the false alarm rate. The threshold is selected to meet the P_{fai} requirements of the individual radiometers. This process is repeated with both signal and noise using the predetermined threshold to calculate the probability of detection. The amplitude of the signal input is set such that the P_{di} requirement of the individual radiometers is met. The signal power-to-noise density ratio is then calculated to give a measure of covertness of the impulse radio system for the single user case.

The covertness value obtained for impulse radio in the single user case is compared with the covertness of wideband and narrowband CDMA systems. For wideband CDMA

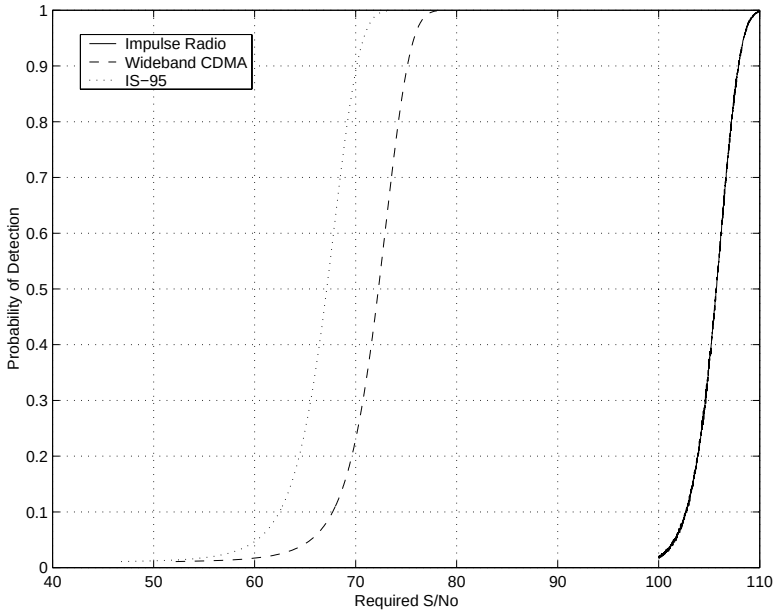

Figure 4.4: Probability of detection, P_d as a function of S/N_0 (dB-Hz) for impulse radio, wideband CDMA and IS-95.

we assume a bandwidth of $B_w = 5$ MHz and a chip rate of 3.6864 Mcps. For IS-95 we assume a bandwidth $B_w = 1.25$ MHz and a chip rate of 1.2288 Mcps. As for the impulse radio system, performance criteria of $P_d = 0.9$ and $P_{fa} = 10^{-2}$ are assumed for these two CDMA systems. The covertness values for these systems are calculated by using Park's model which is suitable for all ranges of time-bandwidth products. The covertness for wideband CDMA and IS-95 in terms of the detectability distance-another measure of covertness is presented in [22]. The results in terms of the required S/N_0 as the measure of covertness used for all the three systems is presented in Table 4.1.

Figure 4.4 shows the variation of the probability of detection P_d with S/N_0 for the three systems. It can be seen from the plot that impulse radio is much more covert than wideband CDMA and IS-95 in the single user case for all performance levels of the radiometer.

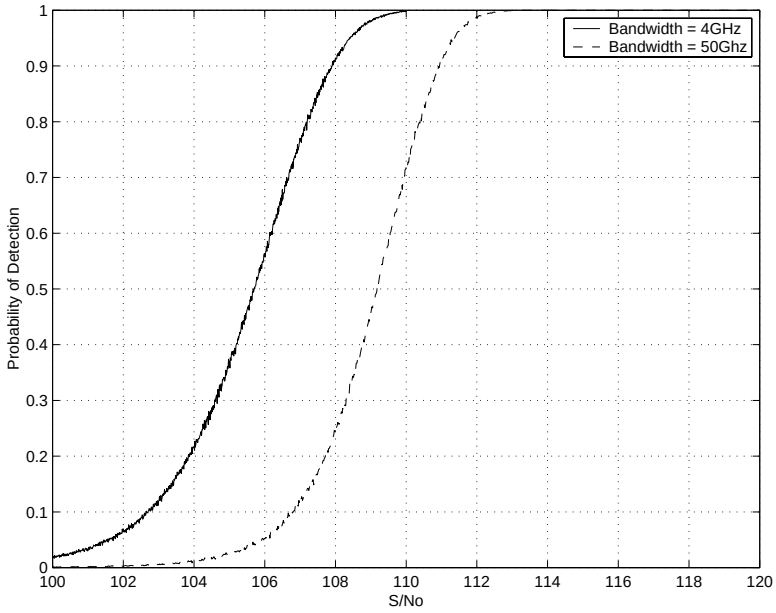

Figure 4.5: Probability of detection, P_d as a function of S/N_0 (dB-Hz) for input filter Bandwidth $B = 4$ GHz and 50 GHz.

4.5.2 Multi-Radiometer Performance with Unknown Bandwidth

In this section we evaluate the performance of the multi-radiometer detector for various values of input filter bandwidth, which would correspond to the detector having no prior knowledge of the impulse radio system bandwidth.The other parameters of the multi-radiometer system are the same as in the optimal case, except that the cutoff frequency for the butterworth filter is modified to match the assigned bandwidth. The P_{di} and the P_{fai} of the radiometer are unchanged from the optimal case because the number of the radiometers per frame interval remain the same since the observation interval is known. Figure 4.5 shows the probability of detect, P_d, as a function of S/N_0 for bandwidth assignments of $B = 4$ GHz and 50 GHz. The increase in bandwidth does not improve signal power but allows more noise power through the filter. However, as seen from the figure, the covertness of the impulse radio system does not increase significantly even for

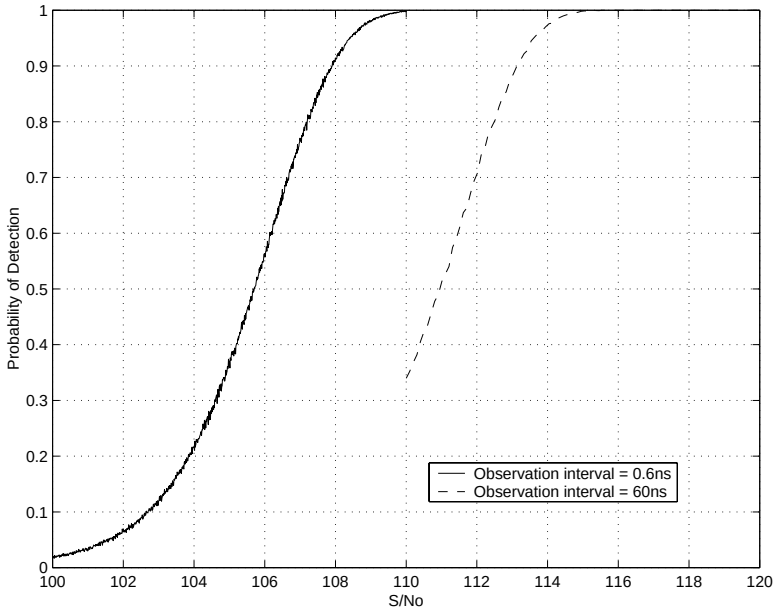

Figure 4.6: Probability of detection, P_d as a function of S/N_0 (dB-Hz) when the observation interval of the radiometer is 6×10^{-10}s and 6×10^{-8}s.

an increase in the noise power by a factor of more than 10. Thus the multi-radiometer performance and hence the covertness are insensitive to filter bandwidth.

4.5.3 Multi-Radiometer Performance with Unknown Pulse Width

Without prior knowledge of the width of the Gaussian monocycle pulse, the observation interval of the multi-radiometer system will be incorrect in general, thus reducing the performance of the multi-radiometer detector. The parameters of the multi-radiometer system are similar to those in the optimal case, but the P_{fai} and the P_{di} change according to (4.11) because the number of radiometers within a single time frame vary with the observation interval. We used the same simulation procedure as before. Figure 4.6 shows a plot of the probability of detect P_d as a function of the S/N_0 for observation intervals of 6×10^{-10} s and 6×10^{-8} s. For the second case, the observation interval equals entire frame

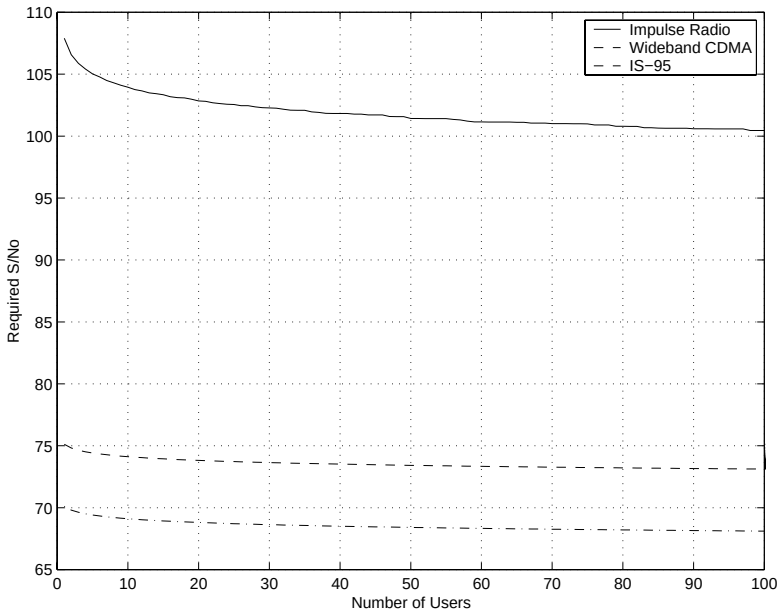

Figure 4.7: Plot of the required S/N_0 (dB-Hz) as a function of the number of users in the non-overlapping pulse case.

time which means that a single radiometer occupies the entire frame. This represents the extreme case when maximum noise power is input to the system. As can be seen from the plot, the covertness for maximum noise input does not change appreciably from the optimal case. It can thus be inferred that multi-radiometer receiver performance and hence the covertness are relatively insensitive to variations of the observation interval.

4.5.4 Multiple Users with Non-Overlapping Pulses

The individual radiometer performance criteria, P_{di}, changes as the number of non-overlapping pulses increase. Since more pulses are present in the system, the individual performance limits can be relaxed according to (4.13). The receiver setup is unchanged from above and the simulation is done for a number user settings. The number of users however cannot increase beyond the number of timeslots in a frame $M = T_f/T_p$ without

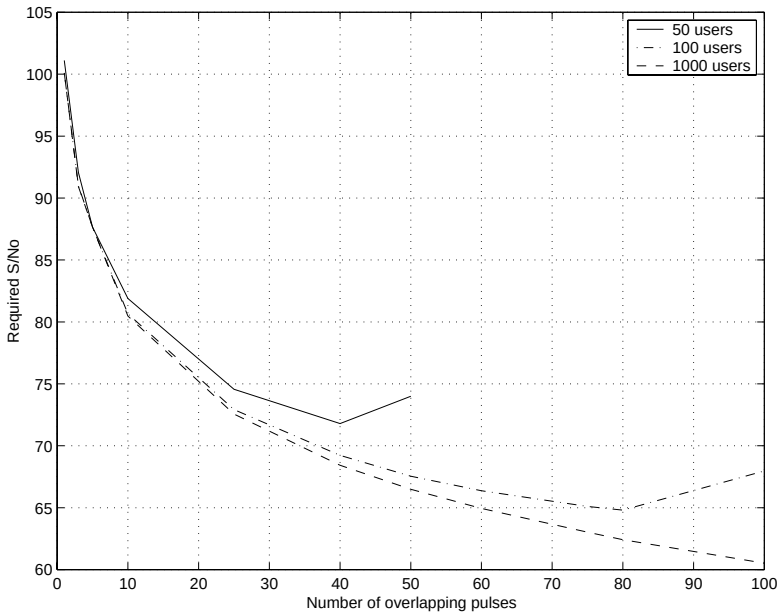

Figure 4.8: Plot of the required S/N_0 (dB-Hz)as a function of number of overlapping pulses, for three different user settings.

overlap. Figure 4.7 shows the variation of the covertness with the number of users. It can be inferred from the figure that although the covertness decreases with the increase in non-overlapping users, the decrease does not significantly affect covertness. When compared with the covertness of wideband and narrow CDMA systems, impulse radio is much more covert even for a large number of non-overlapping users.

4.5.5 Multiple Users with Overlapping Pulses

When the number of active users increase in impulse radio, overlap between the users is inevitable because of the independent pseudorandom sequences of the different users. The amount of overlap varies from frame to frame in a random manner. We assume that when pulses overlap, they do so synchronously i.e., the pulses exactly superimpose upon each other. Partial overlap has a reduced effect on covertness and is not considered. This

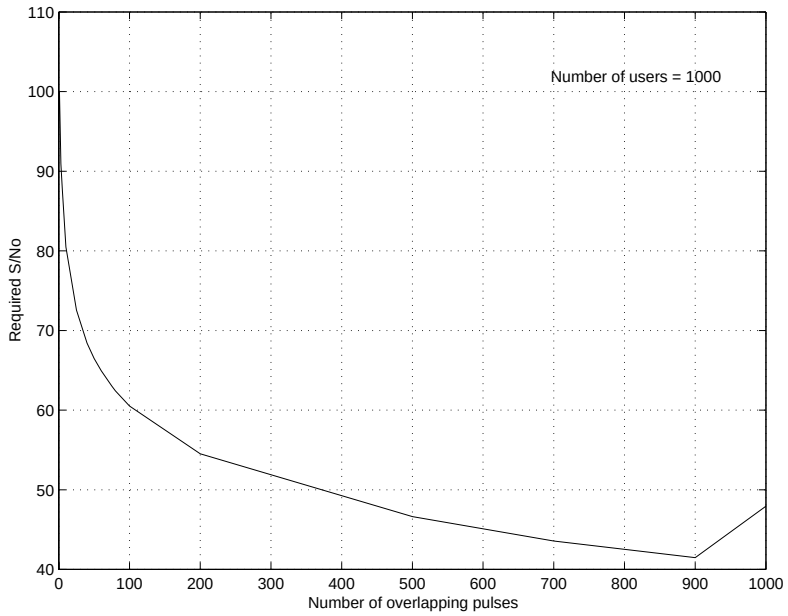

Figure 4.9: Plot of the required S/N_0 (dB-Hz) as a function of the number of overlapping pulses when the number of users = 1000.

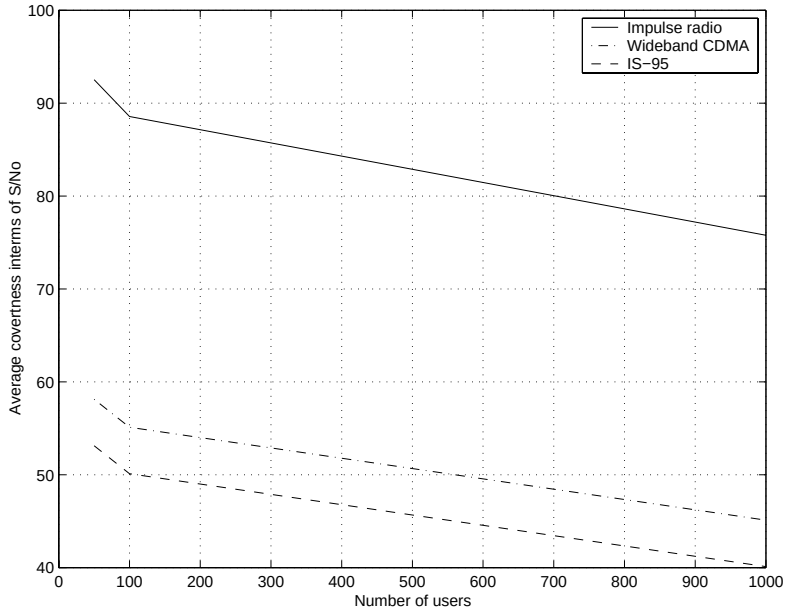

Figure 4.10: Plot of the average covertness in terms of the required S/N_0 (dB-Hz) as a function of the number of users active in the system.

worst-case overlap means that the signal power increases by a factor equal to the number of overlapping pulses in a time slot, since all the pulses are considered to be of equal amplitude. The receiver setup is the same as the optimal multi-radiometer detector, but the performance criteria, P_{di}, for the individual radiometers change according to (4.14). Simulation is used to evaluate performance for different amounts of overlap for a particular number of users and also for different user settings. Figure 4.8 shows plots of the variation of covertness with the amount of overlap for three different user settings. We see from the figure that the covertness decreases as the amount of overlap increases. But, as the number of users that have overlapping pulses increases, the number of timeslots filled within a single frame decreases, thus increasing P_{di} and imposing more restrictions on the performance of the individual radiometers. This can be observed by the upward trend in the plots signifying a slight increase in covertness as large overlap begins to affect the performance limit set for the radiometers. Figure 4.9 shows a more comprehensive variation of covertness for an impulse radio setting of 1000 users, as the number of overlapping users increase to the limit where all the users overlap. The probability of a large overlap occurring is extremely low and thus the covertness on average is much higher than the lower limit obtained by large overlap and also higher than the other CDMA systems.

Given the values of S/N_0 for different overlaps of the multiple user pulses, the average overlap for a particular number of users can be calculated by simulation. The user pulses are uniformly distributed over the timeslots in a single frame and the maximum overlap is found and the corresponding S/N_0 is also determined by interpolating the values already obtained. The average S/N_0 is obtained by repeating this process for a large number of frames. Figure 4.10 shows plots of the average covertness of impulse radio, wideband

CDMA and IS-95 systems for different user settings and it can be seen that the covertness decreases as the number of users increase. In addition, the impulse radio system is seen to be considerably more covert than the other CDMA systems.

Chapter 5

Evaluation of Network Architecture of Impulse Radio

5.1 Introduction

Wireless network architectures can be broadly classified into centralized and distributed systems. Cellular systems conventionally follow the centralized system where the geographical area is divided into cells, each cell serviced by a basestation. The structure is essentially hierarchical wherein a group of basestations is controlled by a basestation switching center (BSC) and a group of BSC's controlled by a mobile switching center(MSC). The basestations perform intra-cellular functions like power control and routing of calls. The BSC handles handovers between basestations and channel assignment among other network functions. The functionality of the MSC includes the management of BSC's, inter-network compatibility and interfacing with landline networks. The survivability of such an architecture in hostile environments is poor because of the concentrated nature of control. The failure of a basestation results in isolation of the mobile

users leaving the network vulnerable. The cellular architecture also suffers from increased deployment time caused by the for a basestation infrastructure and the rigidity of the topology in adapting to changing battlefield conditions.

Distributed packet radio architectures avoid the concentration of functionality into a control center. Distributed architectures have been proposed for military networks in the literature [11][12][13][14]. The functionality is kept at the link level as much as possible with individual links monitoring the transmitter and receiver powers. The nature of packet radio architectures improves the survivability of the network and also allows for rapid deployment and reconfigurability. In a flat packet radio architecture [23][24], nodes are geographically separated into clusters. Within a cluster each node is within a couple of hops from the other nodes in that cluster. A few nodes also form links with nodes in other clusters so as to facilitate inter-cluster traffic. These interconnections between clusters are not rigid and can be re-configured. In a hierarchical packet radio architecture a specific cluster-head is designated which performs inter cluster functionality. these head-clusters can be considered as the second tier in the hierarchy. Despite the hierarchical nature of the cluster-heads, the network remains flexible as cluster-heads are also nodes and the failure of a particular cluster-head results in other nodes assuming cluster-head responsibility.

We have seen that impulse radio is more covert than conventional cellular communication systems. A non hierarchical peer-to-peer topology for impulse radio has been proposed in [9]. In this chapter we evaluate the performance of impulse radio in such a topology by conducting simulations with the developed model and consider modifications to improve covertness. The total power level of the users in such a topology is a criterion along with the power level at an intercepting radiometer.

5.2 Topology Model of a Peer-to-Peer Impulse Radio Network

Conventional packet radio systems suffer from poor covertness and throughput performance due to the high MAC layer signaling overhead due to the stringent acquisition requirements of CDMA. In ultra wideband radio, this overhead becomes much more substantial because it takes longer to acquire the minimum amount of energy required to establish a connection. In impulse radio the increased time is due to the low duty cycle of the Gaussian monopulses. A solution for improving covertness during acquisition periods is proposed in [25] and includes the implementation of Sustained Link Networks (SLN) which reduces net acquisition overhead by maintaining a continuous physical link between two nodes at all times once a logical link has been established between them. The full-duplex nature of impulse radio makes SLN's possible and also increases covertness. These networks maintain the physical connection by transmitting synchronization and power control information during silent periods at low data rates. The signal acquisition and bit synchronization is performed only the beginning of the connection set-up and then the link is maintained. The transmit powers during silent period can be reduced by taking advantage of the increased processing gain. Thus, the interference caused by a silent link on other active links is negligible.

Interference in impulse radio is due to the collision of the Gaussian monopulses of desired and undesired users. Hence users transmitting at high powers results in excessive interference and decrease in overall system performance. This is analogous to the near-far effect in CDMA systems. The effect is mitigated to some extent due to the pseudo-random positioning of the pulses. Cellular systems use centralized power control schemes

to combat the near-far effect [26][27]. In a peer-to-peer network, the functionality of the network is distributed to the links and each links performs power control operations in an independent manner. The performance of these independent link level power control schemes depends on the user density, transmission rates, topology structure and the SNR requirements. To analyze the performance of distributed power control schemes with regard to covertness in an impulse radio network, a simulated network with a peer-to-peer topological structure is required.

A method of simulating random topologies is given in [9] where nodes are randomly created in a specified area and connections are set up between nodes. Links form the connections between two nodes. Multi-node connections are not considered in this thesis. Each generated system is characterized by the triplet $\left(s, \overline{d}, N_t\right)$ where s is the length of a side of a square geographical area where mobile users are deployed. $\overline{d}$ is the average length of the links and N_t is the number of links in the system. $N_u = 2N_t$ as the number of users is twice the number of links. The center for the i^{th} link, (x_{ic}, y_{ic}) are uniform random variables, such that $x_{ic} = U(0, s]$ and $y_{ic} = U(0, s]$. The links are oriented with respect to the sides of the square. The i^{th} orientation is given by $\theta_i = U(0, 2\pi]$. The distance d between the transmitter and the receiver is also a random variable $U\left(0, 2\overline{d}\right]$. However, for analytical reasons which are given in the following sections, the distance is taken to be constant i.e $d = \overline{d}$ for some simulations. The transmitter and the receiver which form the end points of the link are constructed from the link center point, its orientation and the distance between the transceivers. The positions of the transceiver units (α and β) forming the i^{th} link are:

$$\begin{aligned} x_{i\alpha} &= x_{ic} + \tfrac{d}{2}\cos(\theta_i), \quad x_{i\beta} = x_{ic} - \tfrac{d}{2}\cos(\theta_i) \\ y_{i\alpha} &= y_{ic} + \tfrac{d}{2}\sin(\theta_i), \quad y_{i\beta} = y_{ic} - \tfrac{d}{2}\sin(\theta_i) \end{aligned}$$

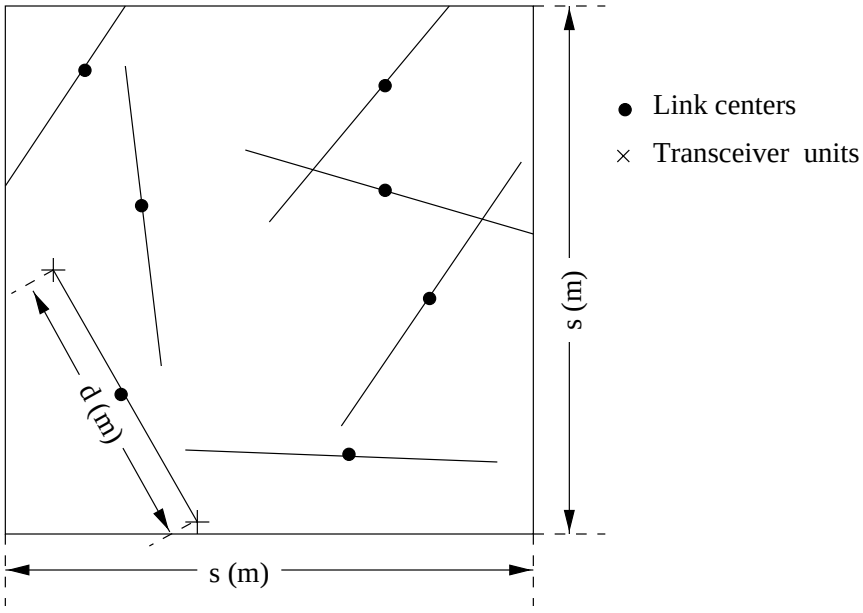

Figure 5.1: Sample topology snapshot based on the described model.

This topology is used as a framework for the network simulations. Figure 5.1 represents a particular configuration of links in the topological network developed using the model described.

5.3 Power Control

Power control ensures that all the users in the network are transmitting at the lowest possible power level in order to improve covertness and capacity. We implement a closed loop distributed power control algorithm presented in [9] over each link while maintaining the desired link quality in the presence of channel variations, mobility, shadow fading and fast fading. Reducing power levels relates to the reduction of multi-user interference in the system and eases the requirements on power supplies.

5.3.1 Background

In most cellular systems, the power control is accomplished by the basestation for the cell that it governs. Downlink power control is implemented to increase capacity and high co-channel interference prompted the use of distributed power control algorithms. Many schemes for distributed power control have been proposed in the literature and can be loosely classified into those that require inter-cellular communication and those that operate on local information alone. A power control algorithm which reduces the global cost measures is proposed in [28] but requires communication between basestations and knowledge about other co-channel links in the network. Distributed power control algorithm operating on local information alone are suggested in [12][29][26].

Similar schemes are also implemented for uplink power control in order to reduce uplink interference to mitigate the near far effects and improve the rate power consumption at the mobile. These schemes equalize the power received at the basestation from all the mobiles [27][30][31]. Fast power control schemes have also been proposed with low feedback delays and which combat the effect of fading in a CDMA system [27][30]. In most of these schemes, the basestations gather the required information through messages sent by the mobile and transmits power control bits to the mobile to adjust its power within physical limitations.

Hierarchical distributed networks employ cluster based power control schemes. The transmit power of all the nodes in the cluster are set to be the same. Power control schemes which depend on both transmission distance and direction are presented in [32]. Adaptive schemes have also been considered which take into account the mobility and shadow fading variances [33]. Since traditional packet radio networks are characterized by short transmission bursts, dynamic closed-loop power control algorithms which com-

pensate for varying channel conditions within a burst are not considered.

5.3.2 A Closed-Loop Power Control Algorithm for Impulse Radio

The topology considered is peer-to-peer and a distributed dynamic power control scheme is implemented. This scheme has been proposed in [9] and has been extended in this work. In impulse radio we consider the links between users to be sustained links where the connection is not terminated even during silent periods and bit rate variations. Since link quality has to be maintained throughout the connection amidst varying channel conditions, a dynamic power control algorithm is implemented. The closed loop feedback based power control scheme is complemented by an open loop power control algorithm during bit rate variations [9].

The power control scheme is based on the signal to interference ratio (SINR) which includes multi-user interference as well as noise. The SINR equation for N_u number of users is derived in [4] . In the topology considered here, the link gains can be computed and individual power levels vary according to power control. A modified version of the equation including link gains is presented in [9].

$$SINR_{i_\beta}(t) = \frac{[A_{i_\alpha}(t)N_{si_\alpha}(t)m_p]^2 g_{i_\beta i_\alpha}(t)}{\sigma_n^2 + N_{si_\alpha}(t)\sigma_a^2 \sum_{j=1, i\neq j}^{N_u}\left[A_{j_\alpha}^2(t)g_{i_\beta j_\alpha}(t) + A_{j_\beta}^2(t)g_{i_\beta j_\beta}(t)\right]} \tag{5.1}$$

The subscript i denotes the i^{th} link, α and β denote the transmitter and the receiver units forming the link, $A_{i_\alpha}$is the amplitude of the pulses transmitted from node α, g_{xy} is the link gain between transmitter x and receiver y where $\{x, y \in (i_\alpha, i_\beta) : i \in [1 \ldots N_l]\}$. The link gains are computer using a simple path loss formula $g_{xy} = d_{xy}^{-\zeta}$ where $d_{xy}^{-\zeta}$ is the

distance of the link or the distance between the two units x and y and ζ being the path loss exponent. N_l is the number of links in the network, m_p is the receiver correlator output for a single pulse, N_s is the number of pulses in one bit, σ_a^2 is the variance of the interfering users and σ_n^2 is the thermal noise power. Using equation 5.1 the signal to interference ratio can be computer at the receiver unit of each link. This quasi-analytical approach allows us to observe the effects of power control without actually simulating the physical link layer of impulse radio.

The SINR is measured at each receiver and the information is fed back to the transmitter in the next cycle. At the transmitter, this information is used to compute the minimum transmit power required to maintain the desired signal-to-interference ratio at the receiver. The information required is local to the link and when each link corrects according to this feedback power control the whole network converges to a steady state. The feedback of the SINR information is continued as the mobile users move. However, since the delay in feedback is low and the convergence rate is high, we assume that the users are stationary for one convergence cycle. The transmit power adjustment is according to the following equation [9]

$$P_{i_\alpha}(t+t_k) = \frac{\gamma_i}{SINR_{i_\beta}(t)} P_{i_\alpha}(t) \tag{5.2}$$

where γ_i is the desired SINR for the i^{th} link, $P_{i_\alpha}(t)$ and $P_{i_\alpha}(t+t_k)$ are transmit powers of the unit α for the i^{th} link at times t and $t+k$, $SINR_{i_\beta}$ is the measured signal-to-interference ratio at the receiver unit β for the i^{th} link. Hence the feedback information is the ratio of γ_i to $SINR_{i_\beta}$. The transmit powers are adjusted by varying the amplitudes of the pulses according to the relation $P_{i_\alpha}(t) \propto A_{i_\alpha}^2(t)$ [9].

We implement a cluster of links in an area as mentioned above and initial transmit

powers are assigned to all the transmitters and the cluster is allowed to converge to a steady state. However, in certain configurations, there are links which do not attain the target S/I ratio even though the transmitters are operating at maximum power. These links are called saturated links and are caused to excessive multi-user interference and high link loss.

5.3.3 Saturated Links

In a topology triplet $\left(s, \overline{d}, N_t\right)$ where the links are deployed randomly and the power control algorithm is initiated, there are some links which do not converge to a steady state. Instead, these links continue to increase the transmitted power till the maximum is reached. In some cases, even when the transmitter power is at maximum strength, the signal-to-interference ratio for effective reception is not attained. These links are called saturated links and they are detrimental to network performance and covertness.

In the topology considered, the interference encountered by a particular link is a function of the other links in the system. Positive interference feedback results in increase in transmitter powers and vice versa. This may spiral out of control resulting in saturated links. An example of saturated links is shown in Figure 5.2 where links A and B are formed by T_A, R_A and T_B, R_B respectively. If T_A increases its transmit power for desired S/I at the receiver, that constitutes an increase in interference at R_B. This increase is fed back to T_B which increases its transmit power and in turn increases the interference at R_A thus forming a spiraling cycle resulting in saturated links.

Saturated links affect covertness by increasing the total power of the network making it vulnerable to interceptors. In a peer-to-peer topology each link monitors its own power and the onset of saturated links can be determined by observing the fluctuations in the

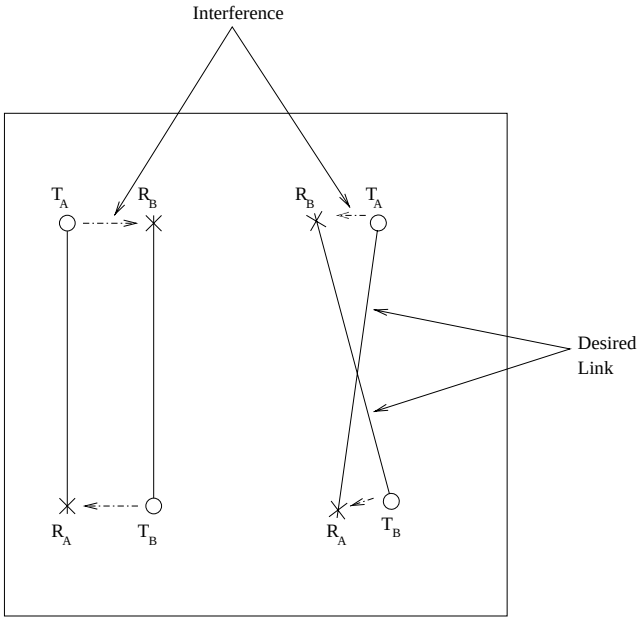

Figure 5.2: Configurations which result in saturated links.

transmit power over a time period. In our simulations we have eliminated saturated links by re-routing the link or eliminating the link. This is essential to reach steady state and also to maintain covertness. Elimination of saturated links can be done in many ways. One way is to inform the cluster-head at the onset of a saturation so that the call can be re-routed to other neighboring links. We have effectively shown that saturated links can be eliminated while still not compromising the communication between the users by shortening the link distance. This is analogous to a handover in cellular systems. Re-routing is difficult in a purely peer-to-peer topology and hence there is a need for a cluster-head to perform functions to maintain network covertness and performance.

5.4 Covertness of a Peer-to-Peer Impulse Radio Topology

In previous chapters we have attempted to quantify covertness of impulse radio by considering a criterion for detection by an interceptor. We considered a radiometer as an interceptor which received impulse radio signals from single and multiple users. In this chapter we examine the power levels generated in a peer-to-peer impulse radio network and consider solutions that increase covertness while maintaining the quality of network communication.

We use the topology triplet $\left(s, \overline{d}, N_t\right)$ explained above along with distributed power control for our simulations. Saturated links are eliminated and steady state power levels are observed. A wideband radiometer is placed in the corner of the square s to evaluate the covertness of the network. The received power at the radiometer is compared with the detection levels for a wideband radiometer calculated in previous chapters. The received power level at the radiometer from all the users in the network constitutes a criterion for quantifying the covertness of a peer-to-peer impulse radio network.

It was shown in 4.5.5 that colliding pulses from multiple users escalate detection probability. In steady state, the detectability depends the distribution of the users in the network and the corresponding transmit power levels. If the user links are too long or the multi-user interference is high, then the transmit powers increase to high levels resulting in ease of detection by an intercepting radiometer. In this chapter we examine the scenarios which result in detectability and consider solutions for enhancing covertness. We consider the worst case scenario where all the received pulses collide which is the single user case. Increased reception at the radiometer and exceeding the covertness

threshold for the radiometer in the corner translates to detection by an interceptor at a distance farther than the corner of the topology square. This is proposed as a criterion for quantifying covertness in [22]. Positioning the radiometer is adequate for this work since we attempt to identify the causes and solutions for controlling detectability with the goal of achieving a network which operates in a covert manner without compromising covertness. The various simulations, results and an architecture currently under analysis which includes a cluster-head into the network topology are given in the next section.

5.5 Simulation Setup and Results

In this section we examine the effectiveness of the peer-to-peer topology and the cases when the covertness of the network deteriorates. We use Monte Carlo simulations to quantify network covertness. We use randomly generated topologies characterized by the triplet $\left(s, \overline{d}, N_t\right)$ as explained in Section 5.2. Given the triplet, the centers of the links are dispersed uniformly through the area and randomly orienting links. Power control is then initiated and saturated are removed as they arise as explained in Section 5.3. Since the feedback delay of the power control is low, the users are assumed to be stationary for the duration of the simulation. The effect of multipath fading is neglected in view of the large system bandwidth.

5.5.1 System Parameters

There is a physical limitation on the maximum amplitude for the transmitted pulses for each link and this is set to be 20 Volts. Power control information is assumed to be transmitted at the next available slot back to the transmitter. Impulse radio employs a

Gaussian monocycle of center frequency $f_c = 2$ GHz and pulsewidth $T_p = 6 \times 10^{-10}$ s. The frame time is 6×10^{-8} s corresponding to $N_s = 256$ pulses per frame. The number of timeslots per frame time interval is $M = 100$ and the bandwidth of the pulse is considered to be $B = 4$ GHz. Using the analysis in Chapter 2 we obtain $\delta = 0.194 \times 10^{-9}$ s, $m_p = 2.7724 \times 10^{-10}$, $\sigma_a^2 = 1.7467 \times 10^{-10}$ and $\sigma_n^2 = 1.14832 \times 10^{-30} \times N_s$. The path loss exponent used is $\zeta = 4$. The desired signal-to-interference ratio for successful decoding of the signal is assumed to be $\gamma = 12$ dB although this can be varied as per quality of service requirements of the mobiles and data quality. A constant bit rate is assumed for all our simulations for comparisons between configurations. The intercepting radiometer is placed at the bottom right hand corner of the given area and has the coordinates $(s, 0)$.

5.5.2 Saturated Links

In each configuration there arise links which do not converge to steady state as explained in Section 5.3.3. In a realistic network the link lengths are random with each link operating independently of the others. A number of such configurations were simulated for varying number of users and the incidence of saturated links was found to increase with the number of users as shown in Figure 5.3. This is due to the increase in multi-user interference due to addition of more users. However, with appropriate re-routing the saturated links can be eliminated as the number of users increase upto a maximum user bound.

Saturated links cause the total transmit power in the network to increase making the network vulnerable to interceptors. Thus, it is essential that these links be re-routed or eliminated from the network.

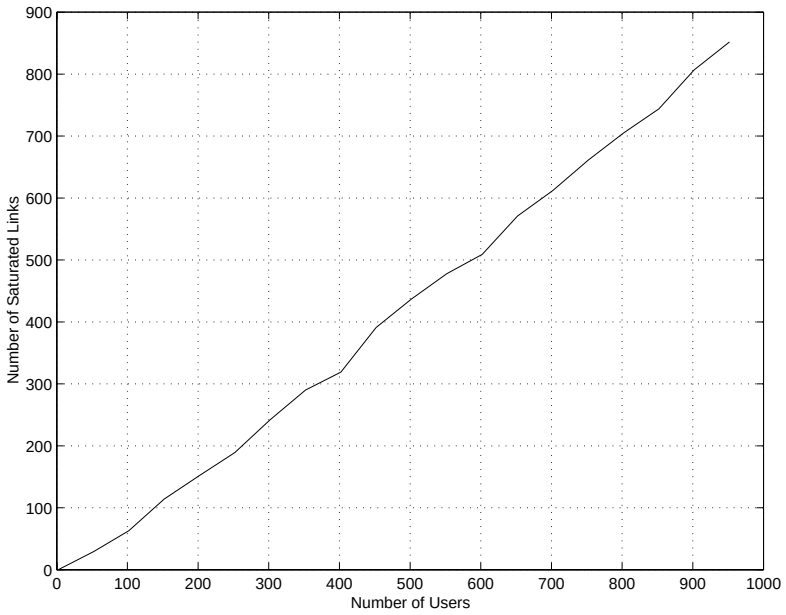

Figure 5.3: The number of Saturated Links as a function of the number of users for a network with random link lengths where $s = 1000$ m and $\overline{d} = 500$ m.

5.5.3 Maximum User Bounds

In a realistic impulse radio network the links between mobile users are of random lengths which vary due to user mobility. For a given area, constant monitoring and re-routing would ensure the absence of saturated links due to the decrease in link lengths. In our simulations we assume a minimum link length of 10 m. Hence, the total number of users for a given area reach a limit at which any further additions of mobile users would result in saturated links. At this point the network is said to be saturated. The number of users required for the saturation of a network depend on the area in which the simulations are conducted.

Figure 5.4 shows the maximum number of users supported as the simulated area increases. As expected the user capacity increases as s increases. User capacity can be defined as the maximum number of users supported at steady state. Steady state is

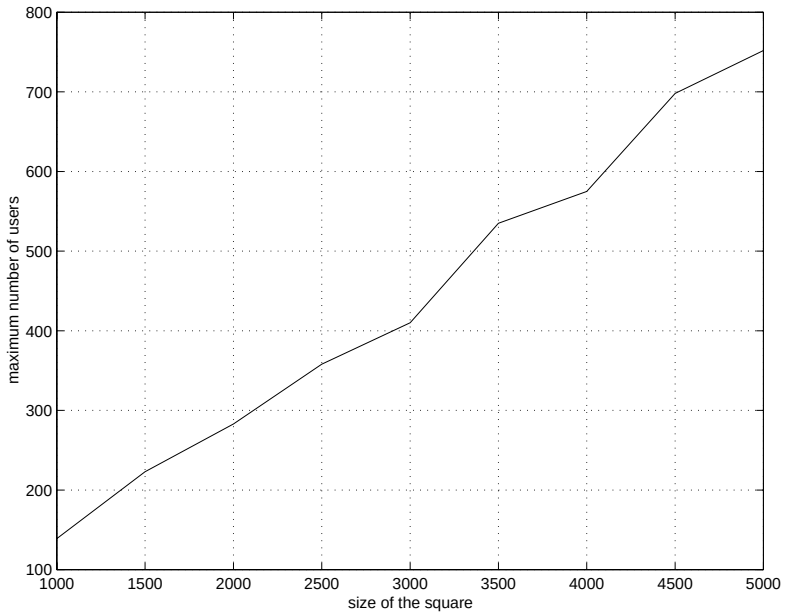

Figure 5.4: The maximum number of users supported as a function of the simulated area where the links lengths are random with a minimum of $d_{min} = 10$ m and $\overline{d} = 500$ m.

attained when all the received powers attain the desired signal-to-interference ratio. In the above simulation, the S/I was taken to be $\gamma = 12$ dB.

Increasing the required S/I or placing tighter constraints on the performance affects the user capacity. Data mobiles which require high quality of service or low probability of error affect increase the desired S/I threshold.

Figure 5.5 shows the decrease in the surviving number of users as the S/I threshold grows more stringent. This is for the topology where $s = 1000$ m with random link lengths with a minimum length of $d_{min} = 10$ m and $\overline{d} = 500$ m.

Another factor limiting the user capacity is the average link length. In a peer-to-peer network, the average link length is constantly varying due to the mobility of the users. At maximum user capacity, an increase in average link length may cause the incidence of saturated links. Hence there is a need for constant monitoring of the network.

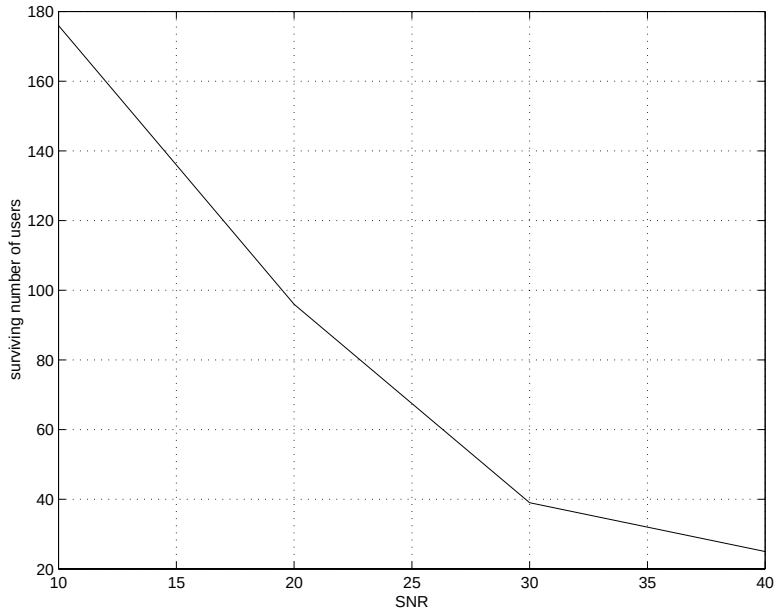

Figure 5.5: The user capacity as a function of the signal-to-interference threshold in a topology with random link lengths with $s = 1000$ m and $\overline{d} = 500$ m.

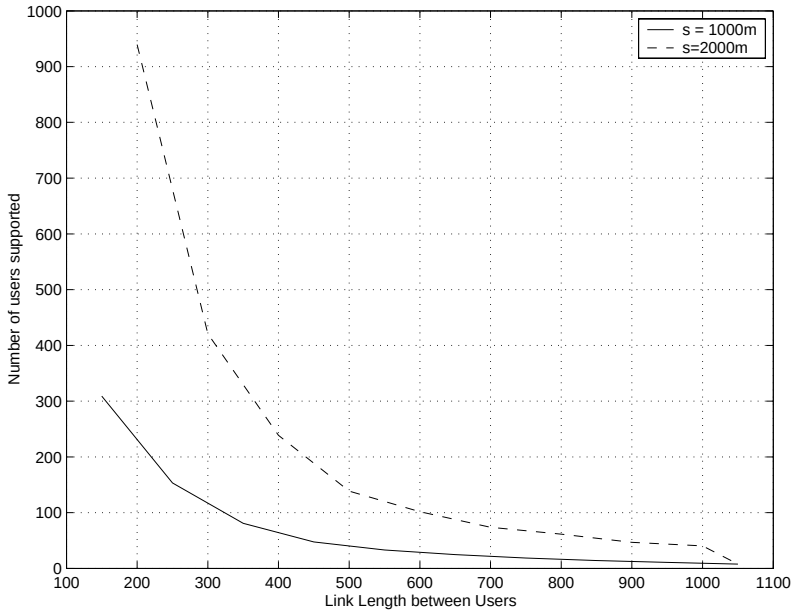

Figure 5.6: The average number of users supported as a function of the link length for different simulation areas.

Figure 5.6 shows the number of users supported as a function of the link lengths of the mobile users. In this simulation, the links lengths are kept constant and the number of users were allowed to converge to a maximum beyond which addition of users would cause saturated links.

These simulations highlight the maximum user capacity bound for a particular simulation area. However, the total steady state power is dependent on both the the link length as well as the total number of users. Thus, satisfying the user bound does not ensure network covertness as discussed in the next section.

5.5.4 Covertness of Peer-to-Peer Impulse radio

A configuration which reaches steady state would have reliable communication across all the links. Given a particular simulation area and a constant number of users within the user capacity, steady state can be easily obtained. However, the position of the users and link lengths determine the covertness of the whole network as they affect the total steady state power. A small number of users operating in a large geographical area with long links would result in reliable communication but a easily detectable system. To avoid the increase in total network power which translates to minimizing the power levels of each cluster, contact monitoring is required.

In our simulations we attempt to quantify the covertness of a topology operating within user bounds. We assume that a network is reasonably covert if it escapes detection by a wideband multi-radiometer placed at the corner of a simulated area.

We use a multi-radiometer as described in Section 4.2.2. To evaluate a covertness bound we consider the worst case scenario where the multi-radiometer has complete knowledge of the system specifications i.e., the pulsewidth and the bandwidth. The

performance criteria for the radiometer is assumed to be $P_d = 0.9$ and $P_{fa} = 1 \times 10^{-2}$. Each one of the M radiometers uses a fourth order Butterworth filter with a 4 GHz cutoff. Since we assume complete knowledge, the observation time period of each individual radiometer is $T_0 = T_p$. The most commonly used criterion for quantifying covertness is S/N_0 [20] which is the required signal power-to-noise power spectral density to meet the detection criteria of the multi-radiometer. The received power at the radiometer in the corner is a result of the constructive combining of the received powers of all the links in the network. Link gains are considered according to a path loss coefficient of $\zeta = 4$.

For a given simulation area with side length $s = 1000$ m, we consider a fixed number of users and evaluate the covertness for different link lengths while keeping within the user bound. Because of the different random processing involved and their inter-dependencies is is a difficult problem to derive a distribution of for the total power level of a network. Hence we use Monte Carlo simulations to observe the effects of power control. Since the variance of the power distribution is high, the figures that are presented are curve fitted using a fourth order polynomial. Since these results should only serve as a bound for the network monitor in order to maintain covertness, curve fitting can be used.

Figure 5.7 shows the curve fitted plot of the received S/N_0 as the link lengths between users vary. The simulation was conducted in an square area of side $s = 1000$ m. The number of users was kept constant at 50. The detection threshold is 107.78 dB and is the threshold for the optimal multi-radiometer as seen in Section 4.5.1. It is evident from the figure that the covertness decreases as the link lengths increase and eventually the received S/N_0 crosses the detection threshold. Constant monitoring is essential to ensure that the threshold is not exceeded. Similar results are obtained for different number of users.

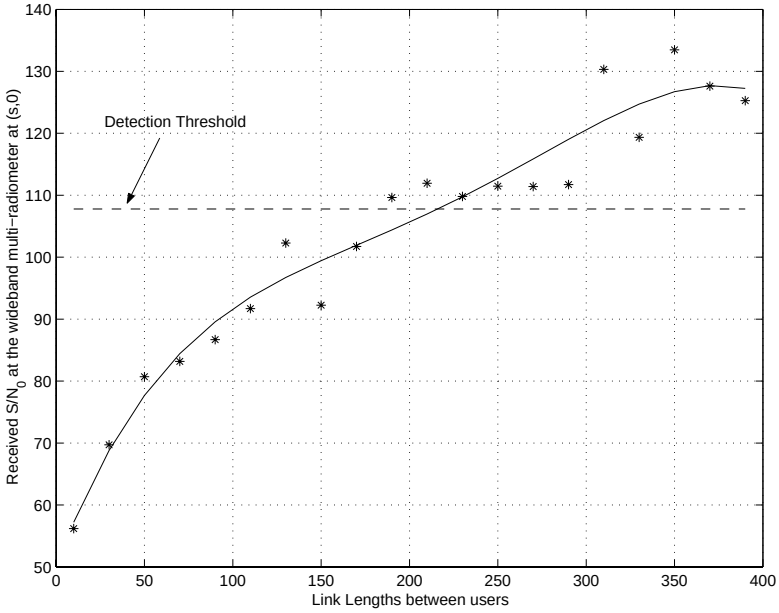

Figure 5.7: Received S/N_0 at the wideband radiometer as a function of the link lengths between users in a network of 50 users in a simulated area with side length $s = 1000$ m. The threshold for detection is 107.78 dB.

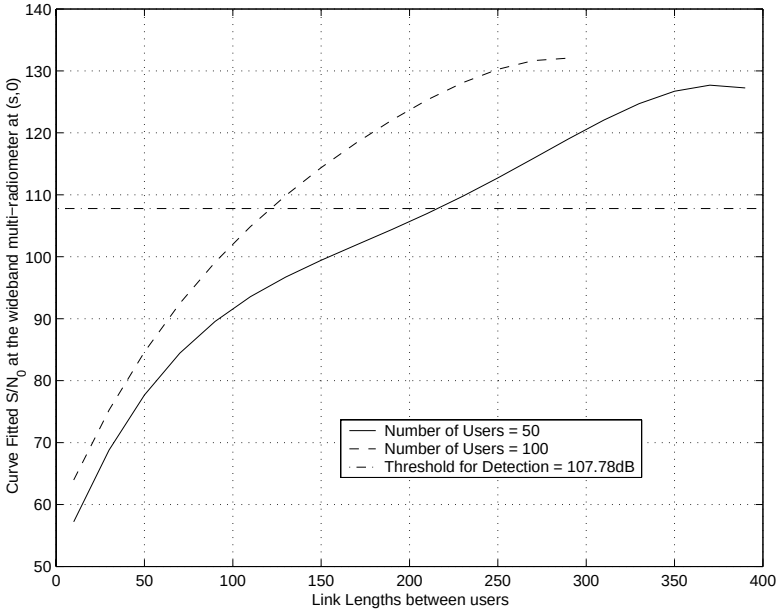

Figure 5.8: Curve Fitted plot of the received S/N_0 values as a function of the link lengths for different user numbers in a network with $s = 1000$ m.

Figure 5.8 shows the curve fitted plots of the received S/N_0 as the link lengths between users vary. Two sets of users are considered in a network where the simulated area is $s = 1000$ m. The S/N_0 for 100 users crosses the detection threshold for a smaller average link length. This is expected because the total power levels are also dependent on the number of users. A network with more users is less covert than a network with lesser number of users. We note from the graph that there is a link length bound for every set of users and this can be considered as a benchmark for the network monitor in order to maintain covertness.

Since the peer-to-peer topology essentially constitutes of distributed independent links which maintain themselves, a network monitor effect is hard to achieve. This is is one of the limitations of this topology.

Chapter 6

Conclusion and Future Work

Impulse radio (IR) is a UWB system that shows promise as a candidate for future tactical military radio networks because of its potential for covert operation and relative immunity to multipath fading. The gain over Commercial-Off-the-Shelf (COTS) systems has to be quantified for evaluating the candidacy of IR. In Chapter 3 we compared the performance of impulse radio and DS CDMA. Conventional narrowband CDMA is modeled as a wideband system which used nanosecond sinusoidal pulses as the mode of information transfer. A single sinusoidal pulse was set to be equivalent to a chip thereby ensuring that the basic characteristics of the modified systems remain the same as standard DS CDMA and thus standard expressions for performance evaluation were used. Comparisons were made with single and multiple users with and without severe local interferers. Impulse radio was found to perform better than DS CDMA for all the cases considered. Better performance translates to higher capacity for a fixed performance criteria and bit rate.

In Chapter 4 we quantify the covertness of impulse radio using a multi-radiometer as the intercepting detector. The multi-radiometer system is developed on the principles of radiometer theory but tailored to detect UWB signals like impulse radio. An

interceptor may have prior knowledge about the communication system which is used to "tune" the detector. Hence the covertness is calculated for different amounts of prior knowledge available to the detector. Worst case covertness bounds are presented since actual covertness is variable and dependent on position and configuration of the users. The covertness measure used is the required S/N_0 for a given performance criteria of the detector. The cases considered include the single and multiple user configurations. Overlapping and non-overlapping pulses were also considered for the multiple user case. Average covertness was calculated for the overlapping case because of the change in covertness on a frame to frame basis. The results show that the detector was insensitive to varying amounts of prior knowledge and the covertness of impulse radio remained relatively constant. Impulse radio was found to be considerably more covert then IS-95 and Wideband CDMA even under worst case conditions. However the covertness was seen to degrade when the number of overlapping users increased.

Chapter 5 examines cases where the covertness of IR degrades and calculates the maximum user capacity for a desired level of covertness. A peer-to-peer topology of impulse radio is used with distributed power control. Saturated links arise as a result of power control and are eliminated by link level monitoring. Results for users uniformly distributed over a geographic area show that covertness degrades when link lengths between users increase. The optimal link lengths were calculated for given user number and desired covertness. It is seen that re-routing decreases link lengths hence increasing the user capacity while maintaining covertness.

Future research should focus on the development of a network topology which maintains covertness while meeting performance and quality of service criteria. Cellular and peer-to-peer topologies have been shown to have limitations in performance at the net-

work level. A quasi hierarchical architecture where cluster-heads perform essential network functions should be considered and a design analysis of its performance should be conducted.

Bibliography

[1] James R. McChesney. Optimization of Tactical Multimedia Networks in the Forward Area. In *Proc. IEEE MILCOM*, pages 1156–1162, 1997.

[2] William J. O'Brien, Jeffrey Seibert, Brian Vogel, and Patricia Young. On Achieving Network LPI for Spread Spectrum Communications. Technical report, E-Systems, Inc., Melpar Division, Oct. 1985.

[3] P. Withington II and L. W. Fullerton. An Impulse Radio Communications System. In H. L. Bertoni, L. Carin, and L. B. Felsen, editors, *Ultra-Wideband, Short-Pulse Electromagnetics*. Plenum Press, 1993.

[4] R. A. Scholtz. Multiple Access with Time-Hopping Impulse Modulation. In *Proc. IEEE MILCOM*, Oct. 1993.

[5] M. Z. Win, R. A. Scholtz, and L. Fullerton. Time-Hopping SSMA Techniques for Impulse Radio with an Analog Modulation Data Subcarrier. In *Proc. IEEE ISSSTA'96*, pages 359–364, Sep. 1996.

[6] Moe Z. Win and Robert A. Scholtz. Comparisons of Analog and Digital Impulse Radio for Wireless Multiple-Access Communications. In *Proc. of the Int. Conf. Commun., ICC' 97*, pages 91–95, June 1997.

[7] M. Z. Win and R. A. Scholtz. Impulse Radio: How It Works. *IEEE Communications Letters*, 2(2):36–38, February 1998.

[8] D. J. Torrieri. *Principles of Secure Communication Systems*. Artech House, 2nd edition, 1992.

[9] S. S. Kolenchery, J. K. Townsend, J. A. Freebersyser, and G. Bilbro. Performance of Local Power Control in Peer-to-Peer Impulse Radio Networks with Bursty Traffic. In *Proc. IEEE GLOBECOM'97*, pages 910–916, Nov. 1997.

[10] J. K. Townsend G. D. Weeks and J. A. Freebersyser. Quantifying the Covertness of Impulse Radio. In *Proceedings of the Ultra Wideband Conference*, Washington D.C., Sept. 1999.

[11] N. Shacham and J. D. Tornow. Future Directions in Packet Radio Technology. In *IEEE INFOCOM Proc.*, pages 93–98, Mar. 1995.

[12] Tsern-Huei Lee and Jen-Cheng Lin. A Fully Distributed Power Control Algorithm for Cellular Mobile Systems. *IEEE J. Select. Areas in Commun.*, 14(4):692–697, May 1996.

[13] J. Sharony. A Mobile Radio Network Architecture with Dynamically Changing Topology Using Virtual Subnets. In *Proc. of the Int. Conf. Commun., ICC' 96*, pages 807–812, June 1996.

[14] L. Williams. Near Term Digital Radio-A First Look. In *Tactical Communications Conference*, pages 423–425, 1996.

[15] Moe Z. Win and Robert A. Scholtz. Ultra-Wide Bandwidth Signal Propagation for Indoor Wireless Communications. In *Proc. of the Int. Conf. Commun., ICC' 97*, pages 56–60, June 1997.

[16] M. Z. Win and R. A. Scholtz. On the Robustness of Ultra-Wide Bandwidth Signals in Dense Multipath Environments. *IEEE Communications Letters*, 2(2):51–53, February 1998.

[17] J. C. Liberti and T. S. Rappaport. Accurate Techniques to Evaluate CDMA Bit Error Rates in Multipath Channels with Imperfect Power Control. In *Proc. IEEE GLOBECOM'95*, pages 33–37, Nov. 1995.

[18] Theodore S. Rappaport. *Wireless Communications, Principles and Practice*. Prentice Hall PTR., 1999.

[19] R. K. Morrow and J. S. Lehnert. Bit-to-Bit Error Dependence in Slotted DS/SSMA Packet Systems with Random Signature Sequences. In *IEEE Transactions on Communications*, pages 1052–1061, Oct. 1989.

[20] R.F. Mills and G.E. Prescott. A Comparison of various Radiometer Detection Models. In *IEEE Transactions on Aerospace and Electronic Systems*, volume 32, pages 467–473, Jan 1996.

[21] D. Norman S. A. Stoops and G. E. Prescott. Simulation of Radiometers for Detection of Spread Spectrum Signals. In *Proceedings of the Tactical Communications Conference*, volume 1, pages 355–368, April 1990.

[22] G. D. Weeks, J. K. Townsend, and J. A. Freebersyser. A Method and Metric for Quantitatively Defining Low Probability of Detection. In *Proc. IEEE MILCOM'98*, Boston, Oct. 1998.

[23] C. R. Lin and M. Gerla. Multimedia Transport in Multihop Dynamic Packet Radio Networks. In *Proceedings of the IEEE International Conference on Network Protocols*, volume 43, pages 209–216, Nov. 1995.

[24] Z. J. Haas. A New Routing Protocol for the Reconfigurable Wireless Networks. In *ICUPC*, pages 562–566, 1997.

[25] S. S. Kolenchery, J. K. Townsend, and J. A. Freebersyser. A Novel Impulse Radio Network for Tactical Military Communications. In *Proc. IEEE MILCOM'98*, Oct. 1998.

[26] Gerard J. Foschini and Zoran Miljanic. A Simple Distributed Autonomous Power Control Algorithm and its Convergence. *IEEE Trans. Vehicular Technol.*, 42:641–646, Nov. 1993.

[27] C C. Lee and R. Steele. Closed-loop Power Control in CDMA Systems. In *IEE Proc. in Commun.*, volume 143, pages 231–239, August 1996.

[28] Shou C. Chen, Nicholas Bambos, and Gregory J. Pottie. On Distributed Power Control for Radio Networks. In *Proc. IEEE ICC*, pages 1281–1285, May 1994.

[29] J. Zander. Distributed Cochannel Interference Control in Cellular Radio Systems. *IEEE Trans. Vehicular Technol.*, 41, Aug. 1992.

[30] Sirikiat Ariyavisitakul and Li Fung Chang. Signal and Interference Statistics of a CDMA System with Feedback Power Control. In *IEEE Trans. Commun.*, volume 41, pages 1626–1634, Nov. 1993.

[31] William C. Y. Lee. Overview of Cellular CDMA. In *IEEE Trans. Vehicular Technol.*, pages 291–302, May. 1991.

[32] Y. Sananda and M. Nakagawa. Power Control Techniques in a Multihop CDMA Packet Radio Network. In *IEEE* 4^{th} *International Symposium on Spread Spectrum Techniques and Applications Proceedings*, volume 3, pages 1162–1166, 1996.

[33] T. Dempsey, C. Langford, R. Martin, and J. McChesney. Evaluation of Adaptive Power Control Algorithms for a Heirarchical Packet Radio Network. In *Tactical Communications Conference*, pages 341–347, 1996.